Torque Measurements of Mass Anisotropy in Pb-Doped $Bi_2\,Sr_2\,Ca\,Cu_2\,O_{8+\delta}$

by

Christopher John Neufeld

A thesis submitted in conformity with the requirements
for the degree of Doctor of Philosophy
Graduate Department of Physics
University of Toronto
April 1996

To my loving wife, Xiao-Yun, for her support, patience, and understanding while I worked on this project, a long way from our home together.

This thesis is also dedicated to the memory of: Roger Chaffee, Georgi Dobrobolsky, Virgil I. (Gus) Grissom, Gregory B. Jarvis, Vladimir Komarov, Christa McAuliffe, Ronald E. McNair, Ellison S. Onikuka, Viktor Patsayev, Judith A. Resnick, Francis R. Scobee, Michael J. Smith, Vladislav Volkov, and Edward H. White II. May we keep their dream alive.

Torque Measurements of Mass Anisotropy in Pb-Doped $Bi_2\,Sr_2\,Ca\,Cu_2\,O_{8+\delta}$

by

Christopher John Neufeld

A thesis submitted in conformity with the requirements
for the degree of Doctor of Philosophy
Graduate Department of Physics
University of Toronto
April 1996

Abstract

We have made measurements of the torque induced by an applied magnetic field of $1T$ on lead-doped $Bi_2Sr_2CaCu_2O_{8+\delta}$ superconducting crystals at liquid nitrogen temperature. Lock-in transitions are detected at doping values of $x = 0.07$ and $x = 0.13$ in $Bi_{2-x}\,Pb_x\,Sr_2\,Ca\,Cu_2\,O_{8+\delta}$, consistent with the predictions of a Lawrence-Doniach model which considers the superconductor as a lattice of superconducting sheets separated by insulating spacers coupled by Josephson tunneling, rather than an anisotropic London model, which treats the superconductor as homogeneous and three-dimensional, with different effective masses m_c and m_{ab} in different directions. We find no evidence of the lock-in transition for $x = 0.30$, suggesting that there has been a crossover to the London regime as a result of the higher level of doping; we cannot reach a definite conclusion in this regard, because the quality of this sample may have been too poor to produce a lock-in. We have examined the Kogan formulation of the anisotropic London model in detail, and have developed a refinement to the theory as it is applied to experimental data. This refinement will force the reevaluation of earlier measurements. We have also obtained values of the superconducting anisotropy factor $\gamma = (m_c/m_{ab})^{1/2}$ for doped and undoped samples; the decrease in γ by an order of magnitude which we observe over the range of doping is consistent with the measured resistivity anisotropies and the Lawrence-Doniach model for these materials.

Acknowledgments

I would like to thank my supervisor, Professor John M. Perz, for his advice and guidance. His swift understanding of problems encountered got me back on track more than once. His patience, understanding, and financial support are appreciated.

I would also like to thank Professor Bryan Statt for his help in defining this work. He suggested this experiment, and also provided invaluable suggestions and advice on laboratory techniques during the day-to-day operation of the experiment. He and his student, Dalibor Kubilek, carried out the measurements of the superconducting transition temperature.

Of course, there could be no results without samples for the experiment. I thank Dr. John J. Neumeier, of the Condensed Matter and Thermal Physics Group MST-10 at Los Alamos National Laboratory, for generously providing the samples used in this work.

I would like to thank Professor Ross Datars of McMaster University for pointing out the possibility of irreversible torque effects due to flux pinning.

Thanks also go to my fellow graduate students for their advice and encouragement. I would especially like to thank Orest Ostapiak for teaching me the procedures of experimental physics in the condensed matter department, from soldering to machining to cryogenics to superconducting magnets; I learned it all from him.

I gratefully acknowledge the financial support of a scholarship from the Natural Sciences and Engineering Research Council, followed by a University of Toronto Open Fellowship, and Professor Perz' NSERC research grant.

Finally, I would like to thank my brilliant wife, Xiao-Yun. She sacrificed much to my thesis work, and provided much-needed emotional and financial support.

Contents

List of Figures

List of Tables

Chapter 1

Introduction

Since the 1986 discovery by Bednorz and Müller [1] of high-T_c superconductivity at 30 K in the perovskite ceramic $La_{2-x}\,Sr_x\,Cu\,O_4$, and the subsequent discovery, by other groups [2] [3] [4], of high-T_c superconductivity at higher temperatures in other copper-oxide-based ceramics, those materials have proven to be a fascinating new challenge in the theory of the mechanisms of superconductivity. In addition to this, though, they have also shown themselves to be a valuable proving ground for conventional theories which explore the ramifications of novel superconducting configurations rather than trying to explain the source of the superconductivity. With different compounds providing superconducting lines and/or sheets along with non-superconducting spacers either larger or smaller than the quantum mechanical length scales of the system, a large variety of theories can be tested in their own regimes. Even leaving aside the as-yet unexplained source of the superconductivity at unprecedented temperatures in high-T_c superconductors, the materials are of great theoretical interest, both in the normal and in the superconducting states.

Through all of the various compositions of the different high-T_c superconductors, a common feature emerges, that of superconductivity confined largely to planes of CuO_2 extending normal to the long axis of the unit cell of a tetragonal or an orthorhombic crystal. Throughout this work we will use the convention that the crystallographic ĉ-axis is perpendicular to the superconducting planes. Aside from untwinned crystals of $Y\,Ba_2\,Cu_3\,O_{7-\delta}$ and $Y\,Ba_2\,Cu_4\,O_8$, which have aligned superconducting chains perpendicular to the ĉ-axis and are beyond the scope of this work, the superconductivity can usually be approximated by an axially-symmetric model, symmetric about the ĉ-axis. It should be noted that there are two different conventions used in the literature of these systems. In one case, the ĉ direction is defined to be the parallel ($\|$) direction; in the other, it is defined to be the perpendicular ($\perp$) direction. We will use the latter, more common convention, in which $\|$ and $\perp$ refer to parallel or perpendicular to the sheets. Because of the ambiguity in the literature, and our attempt to remain consistent in this work, some of our expressions will not appear to match exactly those in the literature. Note also that in all work in the literature, the angle of the applied magnetic field is measured relative to the ĉ-axis, therefore $\theta = 90^o$ corresponds to the case of *parallel* magnetic field.

In all cuprate high-T_c superconducting compounds, particularly in the $Bi_2Sr_2CaCu_2O_{8+\delta}$ and $Tl_2Sr_2CaCu_2O_{8+\delta}$ families, the superconducting behaviour along the ĉ-axis is very different from that along the planes. The large anisotropy in the superconductivity manifests itself in anisotropies of many bulk properties such as critical magnetic field and torque, and is paralleled by anisotropies in normal state properties such as resistivity. This work concerns itself with the anisotropy in the torque experienced by the superconductor in a magnetic field. We will examine two of the theories advanced to predict the torque on an anisotropic or layered superconductor in a magnetic field. In one theory, the superconductors are treated under an anisotropic London model [5], in which the superconductivity extends throughout the entire material, but the effective mass of the carriers is higher along the ĉ-axis than in the plane normal to that axis. In the second theory, the superconductors are treated in a Lawrence-Doniach model [6], in which planes of superconducting material are separated by insulating material, with the planes coupled by Josephson tunneling.

We have examined the London model and have suggested an improvement in the way it is applied to experimental data. We show that an approximation used in the analysis is invalid for highly-anisotropic superconductors, and implement a refinement which produces more accurate results.

We have used a sensitive, low-compliance torquemeter to measure the torque on single-crystal superconducting samples of $Bi_{2-x}Pb_xSr_2CaCu_2O_{8+\delta}$ due to an applied magnetic field, for doping levels $0 \leq x \leq 0.3$, and have examined our measurements in the context of the two models.

The $Bi_{2-x}Pb_xSr_2CaCu_2O_{8+\delta}$ compounds were chosen for this work because, while the degree of anisotropy was known from normal-state resistivity measurements to change significantly from the undoped to the doped materials, other properties, such as the transition temperature, vary little. This shows that these materials can form a very clean experimental system, with few confounding effects due to other changes in physical properties.

In this work we explore the decrease in torque anisotropy of the compound $Bi_{2-x}\,Pb_x\,Sr_2\,Ca\,Cu_2\,O_{8+\delta}$ with increasing lead doping, and look for evidence of a change from two-dimensional to three-dimensional behaviour as the anisotropy becomes very low.

In chapter 2 we present the two most successful and well-developed theories which describe the torque in such systems, the London model adapted by Kogan [5] to the case of anisotropic superconductors, and the Lawrence-Doniach model [6] [7] [8]. We present the reasoning behind the theories, their advantages and disadvantages, and their predictions. We also examine the assumptions of the London treatment and present a refinement to the analysis of data under that model.

In chapter 3 we describe the experimental apparatus, the sample material, sources of error, and the techniques applied to collect the data.

In chapter 4 we present our data, and analyze it in the context of the theories in chapter 2. We compare our conclusions with those of Régi *et al.* [9] from their normal-state resistivity measurements on similar materials.

In chapter 5 we summarize our conclusions and make recommendations for future work in the area.

Chapter 2

Theory

2.1 Kogan's London model treatment

2.1.1 The published theory

Well before the 1986 discovery of high-T_c superconductivity, V. G. Kogan analyzed anisotropic type-II superconductors in the London model [5]. Such materials would have included such materials as artificially prepared layered structures, or certain organic superconductors with a filamentary structure, all with critical temperatures around or below 20 K. It is, therefore, not surprising that his calculation of the torque on such a material [10], published in October of 1988, was the model used most often to fit experimental torque measurements on high-T_c superconductors taken over the following few years.

The London model [11] [12] is a phenomenological two-fluid model of superconductivity. It models the superconductor in terms of a normal fluid which is subject to the scattering mechanisms which result in a finite conductivity in normal metals, and a superfluid current which is not affected by these mechanisms. The model is a local theory, and assumes that the superfluid density does not vary in space [13]. The model itself is a simple one, and does not, for instance, explicitly deal with temperature dependencies, though such dependencies can be incorporated by applying the results of other models to parameters of the London model, imposing a temperature dependence on λ – the London penetration depth – or, equivalently, on n_s – the superfluid density. Despite, or perhaps because of, these shortcomings, it is a useful approach to take for complicated systems which would make a more rigourous analysis, for instance in the Ginzburg-Landau approximation, difficult to perform.

In [5], Kogan presents a generalization of the London equations to the case of anisotropic superconductors. He starts by noting that one can obtain the London equations in the isotropic case by minimizing the energy

$$F = \int [H^2 + (\lambda_0 \vec{\nabla} \times \vec{H})^2] dV/8\pi, \tag{2.1}$$

which is just the sum of magnetic and kinetic energies in CGS units. In Equation 2.1 the penetration depth λ_0 is related to the carrier effective mass by $\lambda_0^2 = c^2 M^\star / 4\pi n_s e^2$. $M^\star$ is the effective mass, and n_s the density, of the superconducting carriers. He goes on to point out that the obvious way to extend the equations to the anisotropic case is to replace $M^\star$ by the mass tensor in a way which keeps the kinetic term invariant:

$$F = \int [H^2 + \lambda^2 (\vec{\nabla} \times \vec{H})_i m_{ij} (\vec{\nabla} \times \vec{H})_j] dV/8\pi. \tag{2.2}$$

Here, $\lambda^2 = c^2 \bar{M}/4\pi n_s e^2$, where $\bar{M}$ is $(M_{xx}M_{yy}M_{zz})^{1/3}$, and m_{ij} are the components of the effective mass tensor divided by $\bar{M}$. Minimization of Equation 2.2 yields

$$H_i = \lambda^2 m_{kl}\, e_{lsi}\, e_{ktj} \frac{\partial^2 H_j}{\partial x_s \partial x_t}, \tag{2.3}$$

where e_{ikl} is the Levi-Civita tensor.

In [14], Campbell, Doria and Kogan compute the free energy density, F, in the uniaxial anisotropic London model. The coordinate system is chosen so that the z direction is parallel to the crystallographic ĉ-axis and the x direction lies along the projection of the magnetic induction on the plane perpendicular to the ĉ-axis, so that $B_y = 0$. The result applies in the broad magnetic field regime in which the applied field H_0 is much larger than the lower critical field, H_{c1}, (typically 100 gauss or 0.01 tesla), and much smaller than the upper critical field, H_{c2}, (typically $>$ 100 tesla); this is the magnetic field regime which will be used throughout this work, unless specifically noted otherwise. The result in [14] is

$$\begin{aligned} 8\pi F &= B^2 + 2H^*(m_1 B_x^2 + m_3 B_z^2)^{1/2}, \\ 8\pi\lambda^2 H^* &\equiv \Phi_0 \ln(\eta H_{c2}/B). \end{aligned} \tag{2.4}$$

where B is the magnetic induction, λ is the average London penetration depth, η is a constant of order unity depending on the flux line lattice structure, $\Phi_0 = \frac{2\pi\hbar c}{2e}$ is the quantum of flux, $m_1 \equiv m_{xx}$ and $m_3 \equiv m_{zz}$ are normalized components of the effective mass tensor along the x and z coordinate axes respectively (see [5]), and H_{c2} is the upper critical field.

Continuing the analysis in [10], Kogan then notes that the field H^* is on the order of H_{c1}, the lower critical field, and is small in comparison with the external field H_0 and the internal fields B and H. By replacing B with H_0 in the logarithm in Equation 2.4 he obtains a theory linear in $H^*/H_0 \ll 1$.

Defining θ to be the angle which the magnetic induction $\vec{B}$ makes with the ĉ or ẑ axis, and substituting

$$m(\theta) = m_1 \sin^2 \theta + m_3 \cos^2 \theta, \tag{2.5}$$

he goes on to compute the thermodynamic field $\vec{H} = 4\pi \partial F / \partial \vec{B}$:

$$\begin{aligned} H_x &= B_x + H^* m_1 m(\theta)^{-1/2} \sin \theta, \\ H_z &= B_z + H^* m_3 m(\theta)^{-1/2} \cos \theta. \end{aligned} \tag{2.6}$$

One can see from Equation 2.6 that the magnetization $\vec{M} = (\vec{B} - \vec{H})/4\pi$ is of order H^*, much smaller than B or H in the magnetic field regimes which we are examining.

Next, Kogan accounts for demagnetization effects for the case of a general ellipsoid,

$$H_{0\alpha} = H_\alpha + 4\pi N_{\alpha\beta} M_\beta, \tag{2.7}$$

where $N_{\alpha\beta}$ is the demagnetization tensor. He calculates the thermodynamic potential of a finite body with respect to the applied field,

$$\tilde{F} = F - \vec{H} \cdot \vec{B}/8\pi - \vec{M} \cdot \vec{H}_0/2, \tag{2.8}$$

and demonstrates that demagnetization imposes a correction on the free energy density proportional to $(H^*)^2$, and hence is unimportant in this approximation in which there are terms proportional to H^*, and in which $\vec{B}$ and $\vec{H}$ are considered to be parallel.

Finally, Kogan calculates the torque in the London model on a uniaxial superconductor of volume V in an applied magnetic field, as a function of the angle θ between the internal magnetic induction and the ĉ-axis, to be

$$\tau(\theta) = -V\frac{\partial \tilde{F}}{\partial \theta} = V\frac{H_0 H^*}{4\pi}\frac{(m_3 - m_1)\sin\theta\cos\theta}{(m_1\sin^2\theta + m_3\cos^2\theta)^{1/2}}. \tag{2.9}$$

The torque in Equation 2.9 vanishes when the magnetic induction lies along the symmetry axis of the material, or in the plane perpendicular to that axis. The direction of the torque is such as to rotate the ĉ-axis to be perpendicular to the applied field. This direction of torque may appear counter-intuitive at first. If one visualizes the superconductor as capable of forming current loops which reside primarily in the plane of low effective mass, one might expect that under an externally applied magnetic induction the screening currents will tend to produce a magnetization which lies along the ĉ-axis, and that this magnetization will then attempt to line up with the externally applied field to produce a torque which aligns the ĉ-axis with the applied field. Such a picture ignores the fact that the penetration length, λ, is larger along the ĉ-axis than in the planes perpendicular to that axis. In this magnetic field regime, the total magnetic flux density across the sample is independent of the orientation of the sample, *i. e.* $\int_S \vec{B} \cdot d\vec{A}/A = const.$ However, the shorter the penetration length perpendicular to the direction of the magnetic field, the smaller the area into which the bulk of the magnetic field is confined. A large penetration depth yields a more uniform magnetic flux density, while a smaller penetration depth yields a higher variation in local field strength, the field being highest at the centres of the flux tubes. As the energy is proportional to the volume density of the square of the magnetic flux B, the orientation which yields the smaller value of the variance of B, $\sigma_B =< B^2 > - < B >^2$, has the lower energy. This orientation is the one in which the magnetic field lines are parallel to the planes.

In experimental analyses it is convenient to express the torque in terms of an anisotropy parameter $\gamma = (m_3/m_1)^{1/2}$. Some algebraic manipulation of Equation 2.9 yields the form used in many experimental papers [7] [15] [16] [17] [18] [19] [20] [21]:

$$\begin{aligned} \tau(\theta) &= AH\frac{\sin 2\theta}{\varepsilon(\theta)} \ln\left[\frac{\gamma\eta H_{c2\perp}}{H\varepsilon(\theta)}\right], \\ \varepsilon(\theta) &= (\sin^2\theta + \gamma^2\cos^2\theta)^{1/2}. \end{aligned} \tag{2.10}$$

where $H_{c2\perp}$ is the upper critical field when applied along the ĉ-axis and $A = \frac{\Phi_0 V}{64\pi^2\lambda^2}\frac{\gamma^2-1}{\gamma^{2/3}}$ is a constant for a given sample, which vanishes when $\gamma = 1$. We should emphasize at this point that the angle θ is still the angle which the magnetic induction internal to the crystal makes with the ĉ-axis. Figure 2.1 shows the form of this torque as a function of angle for various values of γ. Figure 2.2 shows the detail at high angles.

One can use Equation 2.10 to measure the anisotropy of a given sample by determining the value of γ for which the predicted torque maximum occurs at the angle at which the maximum is observed in the sample. The predicted position of the torque maximum is only very weakly sensitive to changes in the parameter $\frac{\eta H_{c2\perp}}{H}$, and variations due to this parameter can be ignored for θ close to 90^o [15]. In Figure 2.3 we plot peak position as a function of γ for $\frac{\eta H_{c2\perp}}{H} = 100$.

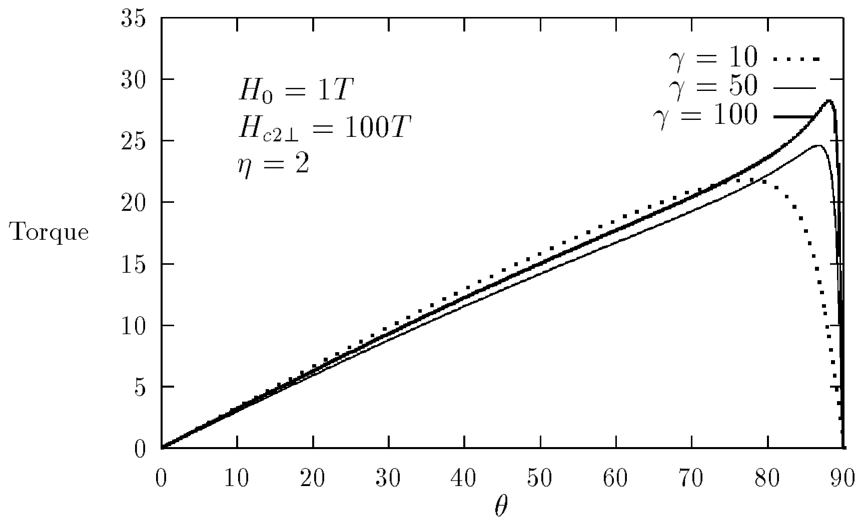

Figure 2.1: Torque vs. angle over entire angular range in Kogan's theory.

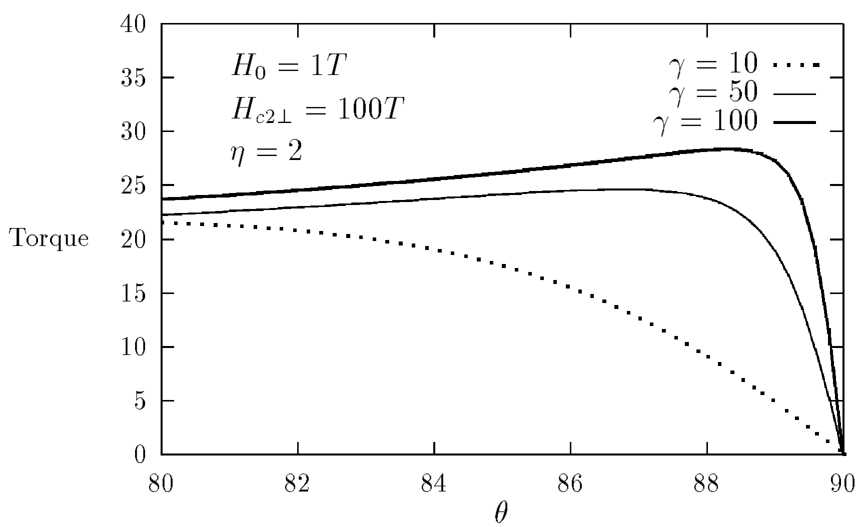

Figure 2.2: Torque vs. angle close to a-b plane in Kogan's theory.

By applying Equation 2.10 to data from various materials, values of γ ranging from 7 to 10 have been inferred for the lanthanum [20] and yttrium [18], [19], [21] compounds, and values as high as nine hundred or more, for the

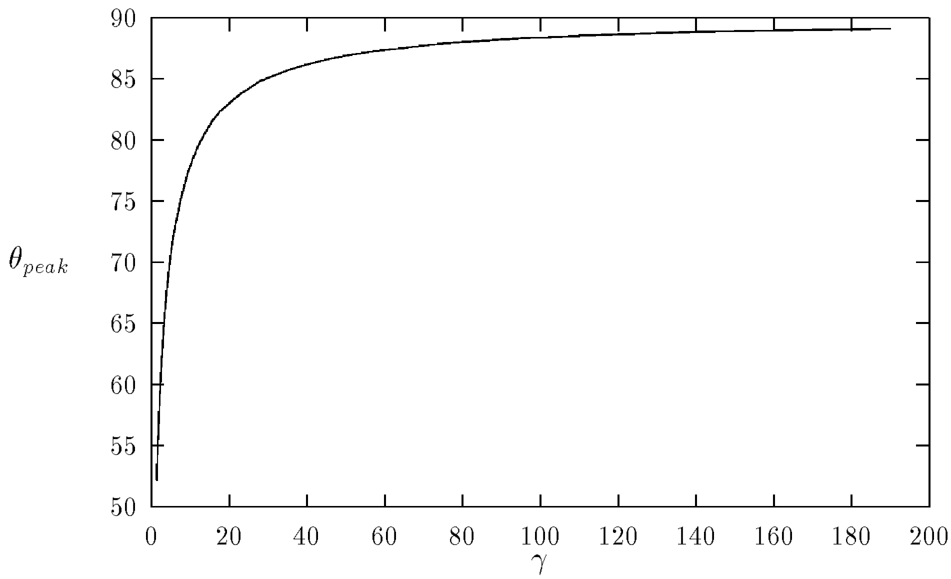

Figure 2.3: Peak position vs. γ in the Kogan-London model, for $\eta H_{c2\perp}/H = 100$

multi-layered bismuth and thallium compounds [15], [17], [22].

2.1.2 A refinement to analysis under Kogan's theory

Leaving aside for now the question of the applicability of the London model to the very highly anisotropic compounds, we believe that the values of γ for those compounds have been artificially inflated in all previous analyses by a failure to consider carefully one of Kogan's approximations in [10].

We will consider the case of an ellipsoid or infinite slab of a high γ superconductor, with the geometric and crystalline symmetry directions coincident, in Kogan's London approximation. In [14], Campbell *et al.* show that the analysis of Kogan in [10] yields the following expression from which we can infer the magnetization:

$$\begin{aligned}H_z &= B_z + \tfrac{\eta\Phi_0}{2\lambda^2}\tfrac{m_3 B_z}{B\sqrt{m_{zz}}}\ln\left[\tfrac{H_{c2}}{B}\right],\\ H_x &= B_x + \tfrac{\eta\Phi_0}{2\lambda^2}\tfrac{m_1 B_x}{B\sqrt{m_{zz}}}\ln\left[\tfrac{H_{c2}}{B}\right].\end{aligned} \tag{2.11}$$

Exploiting this result, and recalling that $\vec{H} = \vec{B} - 4\pi\vec{M}$, we see that it is not always true that applied magnetic field, $\vec{H}_0$, and the internal magnetic induction, $\vec{B}$, are parallel to the degree required to approximate θ as the angle of the applied magnetic field. In the case of high anisotropy parameter γ, and for θ close to 90^o, the departure is important, and impacts significantly on the inferred value of γ.

For large anisotropies, the magnetization, $\vec{M}$, is strongly directed along the ĉ-axis, even when the applied field is almost perpendicular to that axis. Campbell *et al.* show [14] that

$$\frac{M_x}{M_z} = \frac{m_1}{m_3}\frac{B_x}{B_z} = \frac{1}{\gamma^2}\frac{B_x}{B_z} \tag{2.12}$$

Recall that the superconductor is a diamagnet, so the direction of magnetization is more than 90^o away from the direction of the applied magnetic field, and tends to reduce B_x and B_z from their values in the absence of a diamagnetic response. We can see from Figure 2.1 that it is exactly in the high angle measurements that the anisotropy makes itself noticed, and that any discrepancy between the θ of the theory and the θ of the experiment in the high angle region will compromise the value of γ inferred from the experiment. Indeed, according to Kogan's model, in the very high angle region at high anisotropies the z-component of the magnetization can be comparable to that component of the applied field.

It is possible to apply a first-order correction in order to estimate the impact of this effect on measurements of γ. We can solve Equation 2.11 self-consistently with

$$\vec{B} = \vec{H}_0 + 4\pi(\mathbf{I} - \tilde{N})\vec{M} \tag{2.13}$$

for particular values of γ, H_0, θ_0 (the angle which the applied magnetic field makes with respect to the crystal axis), H_{c1}, H_{c2}, and $\tilde{N}$ – the demagnetization tensor. This solution yields values of θ, $\vec{B}$, $\vec{H}$, and $\vec{M}$. In Figure 2.4 we plot the discrepancy between θ and θ_0 in the high-angle region for different anisotropies, assuming a large, flat crystal, and neglecting edge effects ($N_{zz} = 1, N_{xx} = N_{yy} = 0$). Note that the angle which the magnetic induction makes with the ĉ-axis is smaller than that which the applied magnetic field makes. A peak which occurs at a certain θ_0 actually corresponds to a smaller value of θ inside the crystal.

We can now pick values of γ, apply Equation 2.10 to obtain the torque spectra predicted for those values, then use the procedure detailed above to extract a corrected value of γ. Table 2.1 contains some results of such an analysis. We note that the effect is minor at low anisotropies, staying within the error bars of typical experiments [18]. At higher anisotropies the effect is much too large to be ignored.

We should point out that this is only a first-order correction to the earlier results, as we have applied these corrections to Kogan's equations, which already contain the incorrect assumption. As Equation 2.11 is derived by Campbell *et al.* using the simplification that B and H_0 are parallel, our use of

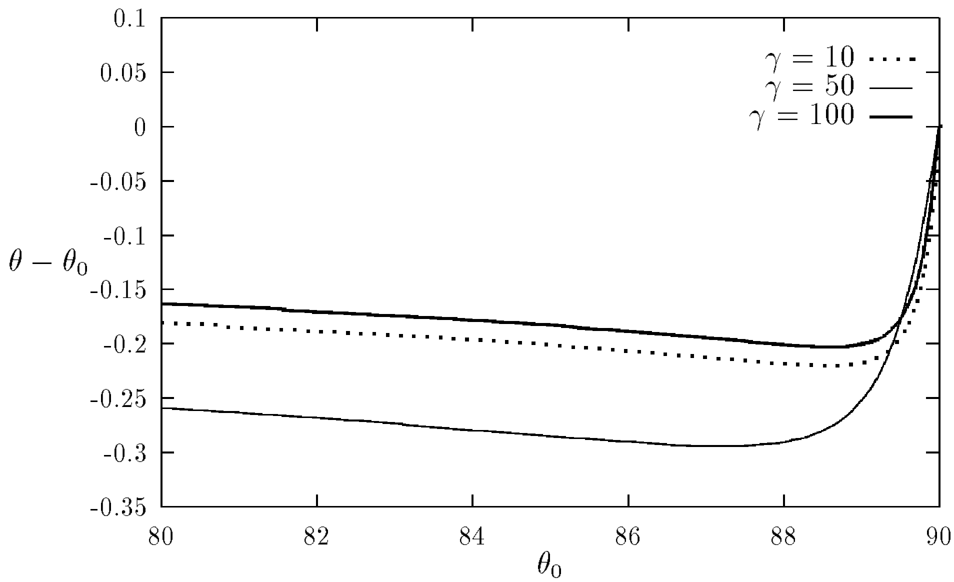

Figure 2.4: Magnetization correction: $\theta - \theta_0$ vs. θ_0 in degrees

Old γ	New γ	Compound
7.9	7.54	$Y\,Ba_2\,Cu_3\,O_{7-\delta}$[18]
55	49.4	$Bi_2\,Sr_2\,Ca\,Cu_2\,O_{8+\delta}$[15]
106	54.0	$Bi_2\,Sr_2\,Ca\,Cu_2\,O_{8+\delta}$[21]
220	102	$Bi_2\,Sr_2\,Ca\,Cu_2\,O_{8+\delta}$[21]

Table 2.1: Effect of demagnetization correction on some values of γ

this equation to show that the fields are not negligibly divergent can only be justified as a first-order correction.

We believe that torque anisotropy measurements for highly anisotropic superconductors should be reanalyzed in light of this finding. This will result in a significant lowering of the published γ values for all of these materials.

Historically, all estimates of γ obtained from torque measurements in the literature have been obtained by fitting to the Kogan-London model. Even those materials which have since been shown to be better described by a

Lawrence-Doniach model will probably continue to be analyzed in the Kogan-London model until such time as a formalism for analysis under the Lawrence-Doniach model becomes available. In the interim, a reanalysis, in light of our work, of the earlier results using the Kogan-London model is important.

2.1.3 Shortcomings of a London treatment

As noted earlier, the London theory has been widely used in analyses of experimental torque data to date. In fact, evidence is that the model may be sufficient over some temperature ranges for some of the low anisotropy materials such as $Y\,Ba_2\,Cu_3\,O_{7-\delta}$ and $La_{2-x}\,Sr_x\,Cu\,O_4$, and may be valuable at higher fields (above two tesla) for other materials [22]. Even in relatively low anisotropy materials such as $Y\,Ba_2\,Cu_4\,O_8$ there is evidence [23] that a homogeneous model fails to account for the behaviour of the ĉ-axis penetration depth. Furthermore, Shibauchi *et al.* [24] have measured the temperature dependence in $La_{2-x}\,Sr_x\,Cu\,O_4$ of $\lambda_{||}$ and $\lambda_{\perp}$, the penetration depths in the directions parallel and perpendicular to the superconducting planes, respectively, and have concluded that the material behaves in a way which can be best explained by a Josephson-coupled layer model. There is ample evidence now that a more detailed model is necessary to explain all of the properties of the high anisotropy materials.

The anisotropic London model treats the superconductor as a homogeneous material with no small-scale structure. Consequently, the superconducting order parameter does not vary within the material. The penetration depth or effective mass is assumed *a priori* to be anisotropic, and the consequences of this assumption are explored. The layered cuprate superconductors, though, are not homogeneous along the symmetry axis. Superconductivity in these materials resides largely in the CuO_2 planes, so that the materials more closely resemble a lattice or superlattice of superconducting sheets in an insulating or normal metal matrix. When the ĉ-axis coherence length in the superconductor falls below the repeat spacing of the lattice, the London model with its uniform superfluid density breaks down.

2.2 Lawrence-Doniach model

2.2.1 The model in the quasi-2D regime

In this work we have been concerning ourselves with anisotropic superconductors, in particular the high-T_c superconductors. As noted earlier, these materials are characterized by superconducting sheets separated by insulating layers, all of which are perpendicular to the ĉ-axis of the crystal.

In the case that the coherence length in the ĉ-direction, ξ_c or $\xi_\perp$, is smaller than the thickness of an insulating layer, an analysis which treats the material as intrinsically three-dimensional, such as the Kogan-London model of Section 2.1, breaks down. The simplest approach which can handle such a situation is the Lawrence-Doniach model [6]. In this model, Lawrence and Doniach treat superconducting sheets separated by insulating layers and coupled by Josephson tunneling.

A good review of this case is provided in [25]. The Lawrence-Doniach model considers an SIS (superconducting-insulating-superconducting) model, a simple alternation of superconducting and insulating layers. The Lawrence-Doniach free energy functional is given ([8], [25], [26]) by

$$\begin{aligned} F &= d\sum_n \int_{sheet} \left[a(T)\left|\Psi_n\right|^2 + \frac{1}{2}b\left|\Psi_n\right|^4 + \frac{\hbar^2}{4M}\left|(\imath\vec{\nabla}_{\parallel} + \frac{2e}{\hbar c}\vec{A}_{\parallel})\Psi_n\right|^2 + \right. \\ & \left. \frac{\hbar^2}{4M'd^2}\left|\Psi_{n+1} - \Psi_n \exp(\frac{2\imath e}{\hbar c}\int_{nd}^{(n+1)d} A_z\, dz)\right|^2 + \frac{H^2}{8\pi}\right] d^2\vec{r} \end{aligned} \tag{2.14}$$

In Equation 2.14, d is the distance between sheets, n counts over the superconducting sheets, $a(T) = a_0(T - T_c)$ and b are energy parameters of the Lawrence-Doniach model with $a_0 > 0$, Ψ_n is the superconducting wavefunction in plane n, $\vec{A}$ is the electromagnetic vector potential, M is the effective mass in the sheets, M' is an effective phenomenological mass given by $M' = \frac{\hbar^2}{4d^2\tilde{\eta}}$ with $\tilde{\eta}$ as the Josephson tunneling parameter, and V is the volume of the sample.

If the perpendicular coherence length, $\xi_c(T) = \sqrt{\hbar^2/4M'|a(T)|} \ll d$, the distance between sheets, the Lawrence-Doniach equations can be simplified by setting $|\Psi_n| = \Psi_0 = \sqrt{|a(T)|/b}$. This is certainly the case for the higher anisotropy high-T_c superconductors except immediately below T_c where ξ_c diverges. Kes *et al.* estimate [27] that this is true for $Bi_2\,Sr_2\,Ca\,Cu_2\,O_{8+\delta}$ when $T_c - T \gtrsim 0.5\ K$.

2.2.2 Field parallel to the layers

Under this model, when a magnetic field is applied parallel to the layers, at $\theta = 90^o$ in our notation, an anisotropic Abrikosov lattice of flux vortices is formed. The vortices are centred on the insulating sheets to minimize the free energy, and have Josephson cores in which the superconducting order parameter does not vanish anywhere in the structure, rather than the more usual Abrikosov cores. This state is referred to as the "transparent state" [26] or the "locked-in state" [8], [25]. As the latter is the more common term, we will use it in what follows.

The free energy density in this geometry is given ([8], [25], [28]) by

$$F_{\|} = \frac{B^2}{8\pi} + \frac{\Phi_0 B}{(4\pi\lambda_{\|})^2\Gamma}\left[\ln\sqrt{\frac{H_0}{B}} + \alpha_J\right], H \ll H_0. \tag{2.15}$$

Here, $H_0 = \Phi_0/\pi\Gamma d^2$ is the field at which the ĉ-direction vortex spacing becomes equal to d. $\Gamma = \sqrt{M'/M}$ is capitalized to distinguish it from γ used similarly in Kogan's London model described in Section 2.1. α_J is a correction to the logarithm due to overlap between the nonlinear cores. Bulaevskiĭ [28] estimates $\alpha_J \simeq 1$. Clem *et al.* have calculated [29] that, for a single flux vortex, $\alpha_J = 1.12$.

2.2.3 Tilted magnetic field

For magnetic fields applied at angles other than $\theta = 90^o$, the vortices can appear in one of four forms [8]. Whether all forms are present depends on whether $H_{c1\perp}$ is greater or lesser than $H_J = \frac{\Phi_0}{4\pi\lambda_{\|}^2}\ln\frac{\lambda_J}{\xi_{\|}}$, where $\xi_{\|}$ is the in-plane coherence length and λ_J is the Josephson length [30]. For high-T_c superconductors, in which the thickness of the superconducting layers is much smaller than the penetration depth $\lambda_{\perp}$, we can simplify $\lambda_J = \Gamma d$ [30]. The possible forms of the vortex lattice are:

I – The Meissner phase. No flux lines penetrate the sample.

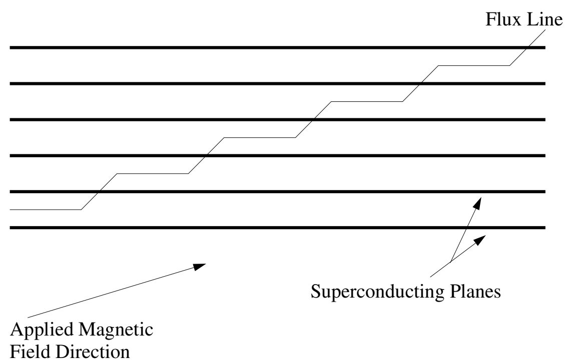

Figure 2.5: A staircase flux vortex

II – The flux lines can be straight, forming an angle φ to the $\hat{c}$-axis.

III – The flux lines can form a staircase shape, with straight segments running along the insulating layers, then tilting to cross a superconducting sheet over a length ([8]) of roughly λ_J (see Figure 2.5). This phase is present only when $H_J > H_{c1\perp}$.

IV – The flux vortices can remain in the locked-in state described in Subsection 2.2.2.

Phase diagrams for $H_J > H_{c1\perp}$ and $H_J < H_{c1\perp}$ are shown in Figures 2.6 and 2.7 respectively. These diagrams are adapted from figures in Ref. [25], which are in turn inspired by similar diagrams in Ref. [8].

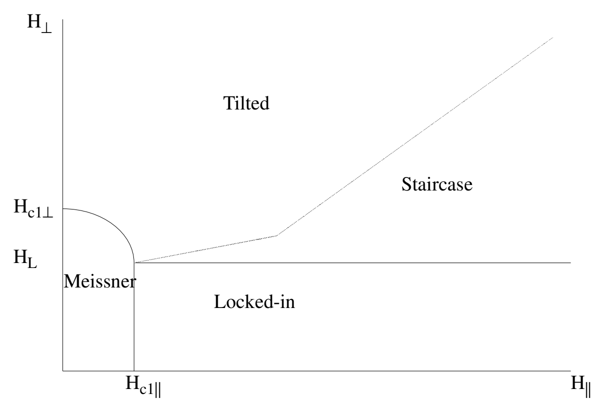

Figure 2.6: Phase diagram of the vortex configuration in the Lawrence-Doniach model for $H_J > H_{c1\perp}$. The diagram is adapted from Reference [25].

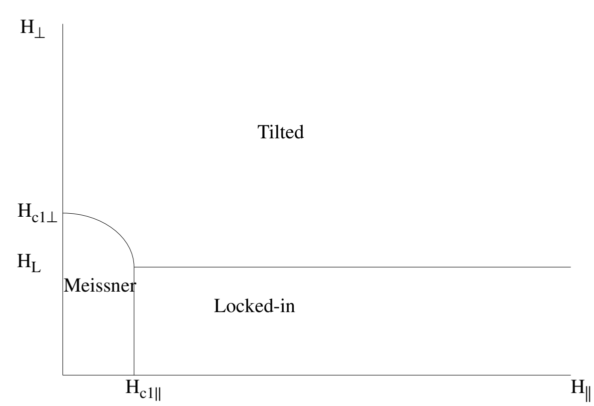

Figure 2.7: Phase diagram of the vortex configuration in the Lawrence-Doniach model for $H_J < H_{c1\perp}$. The diagram is adapted from Reference [25].

The free energy of case II, in the case of $\tan\theta \ll \Gamma$ (and consequently $\theta \approx \varphi$), is given by [25]

$$\begin{aligned} F(\varphi) &= \tfrac{B^2}{8\pi} + \tfrac{\Phi_0 B}{(4\pi\lambda_{||})^2}\varepsilon(\varphi)\ln(\sqrt{\tfrac{\Phi_0}{\pi d^2 \tan^2\varphi\varepsilon(\varphi)B}}) + \tfrac{\Phi_0 B_\perp}{(4\pi\lambda_{||})^2}\left[\ln\tfrac{d\tan\varphi}{\xi_{||}} + \alpha_{2D}\right], \\ \varepsilon(\varphi) &= \sqrt{\cos^2\varphi + \Gamma^{-2}\sin^2\varphi}. \end{aligned} \tag{2.16}$$

The free energy of case III, for $\tan\theta > \Gamma$, becomes [25]

$$F = \frac{B_{||}^2}{8\pi} + \frac{\Phi_0 B_{||}}{(4\pi\lambda_{||})^2\Gamma}\left[\ln\sqrt{\frac{H_0}{B_{||}}} + \alpha_J\right] + \frac{\Phi_0 B_\perp}{(4\pi\lambda_{||})^2}\left[\ln\frac{\min(\lambda_{||},\Gamma d)}{\xi_{||}} + \alpha_{2D}\right]. \tag{2.17}$$

In these expressions, α_{2D} is the core energy, in units of $\frac{\Phi B_\perp}{(4\pi\lambda_{||})^2}$, of a single 2D vortex. For $d \ll \lambda_{||}$ this is close to the 3D value, $\alpha_J \approx 1$ of Equation 2.15 [28], [29].

2.2.4 The lock-in transition

Following the treatment of [25], we can apply $G = F - \vec{H}\cdot\vec{B}/4\pi$ and Equation 2.17 to show that as the direction of the applied field approaches that of the planes, the flux vortices move continuously to become aligned with the planes, even when the externally applied field is not aligned this way (see Figure 2.6). This occurs at

$$H\cos\theta_L = H_L,\ H_L = \frac{\Phi_0}{4\pi\lambda_{||}^2}\left[\ln\frac{\min(\lambda_{||},\Gamma d)}{\xi_{||}} + \alpha_{2D}\right]. \tag{2.18}$$

Note that as H increases, the lock-in transition appears at angles closer and closer to $\theta_L = 90^o$. In order to resolve the lock-in transition, then, intermediate fields are desirable.

In Equation 2.18, H is the internal magnetic field. Demagnetization effects complicate the issue. At the lock-in transition the following is true [25]:

$$H_{0z} = H_z + 4\pi n_z M_z = (1 - n_z) H_z \qquad (2.19)$$

This leads immediately to:

$$\cos\theta_{0L} = (1 - n_z)\cos\theta_L \qquad (2.20)$$

Here, H_0 is the applied magnetic field, forming an angle θ_0 to the ĉ-axis of the sample, and H is the magnetic field internal to the sample, forming an angle θ to the ĉ-axis of the sample. For plate-like or thin-film samples, with $n_z \lesssim 1$, the angle of the applied field at which the lock-in transition appears is extremely close to $\theta_0 = 90^o$. This makes the lock-in undetectable in such samples, and explains the absence of this transition in some data from torque measurements of $Bi_2\,Sr_2\,Ca\,Cu_2\,O_{8+\delta}$ or $Tl_2\,Sr_2\,Ca\,Cu_2\,O_{8+\delta}$ samples ([15], [17], [21]). Other measurements ([7], [22]) on plates with less severe aspect ratios have demonstrated this transition in undoped $Bi_2\,Sr_2\,Ca\,Cu_2\,O_{8+\delta}$ and $Tl_2\,Sr_2\,Ca\,Cu_2\,O_{8+\delta}$ at intermediate fields (below $0.5T$ and $1.0T$ respectively).

For our samples, with aspect ratios of approximately 1/5, $n_z \approx 0.77$ [31], so Equation 2.20 produces an estimate for $\theta_{0L} \approx 89.5^o$. When searching for the lock-in transition in our samples, therefore, we will exclude from consideration any features for $\theta < 89^o$.

This lock-in transition has no analogue in the Kogan-London model, and so forms a very clear signature of the failure of the Kogan-London model. It is characterized by an anomalous increase in the torque followed by a discontinuous change in slope, and a linear decrease to zero torque at $\theta = 90^o$.

As our samples are fairly thick, we expect to see this transition at least in the low doping samples, if, as we expect, the Lawrence-Doniach model is more appropriate than the Kogan-London model.

2.2.5 Torque predictions of Lawrence-Doniach model in the quasi-2D regime

For low angles, $\tan\theta \ll \gamma, \Gamma$, the Lawrence-Doniach model and the Kogan-London model of Section 2.1 predict the same torques, and we can use Equation 2.10 in this neighbourhood. Once again, the torque in this model is directed so as to align the superconducting sheets with the applied magnetic field. In this case this is because of the energy cost associated with puncturing a superconducting sheet with a magnetic flux line. It is much more energetically favourable to allow the flux lines to concentrate themselves as much as possible in the non-superconducting spacers, hence the torque aligning the spacers with the applied field.

At higher angles, the torque in the Lawrence-Doniach model departs from that of the anisotropic Kogan-London model. A more general treatment is given by Bulaevskiĭ [32], to yield torques in the locked-in phase

$$\tau(\theta) = A\frac{4\pi\lambda_{\|}^2 H}{\Phi_0}\cos\theta. \tag{2.21}$$

The intermediate region, at moderately high angles but before the lock-in transition, has not been solved in any closed form. A numerical solution to the free energy equations has been done by Steinmeyer [7], and his plots are

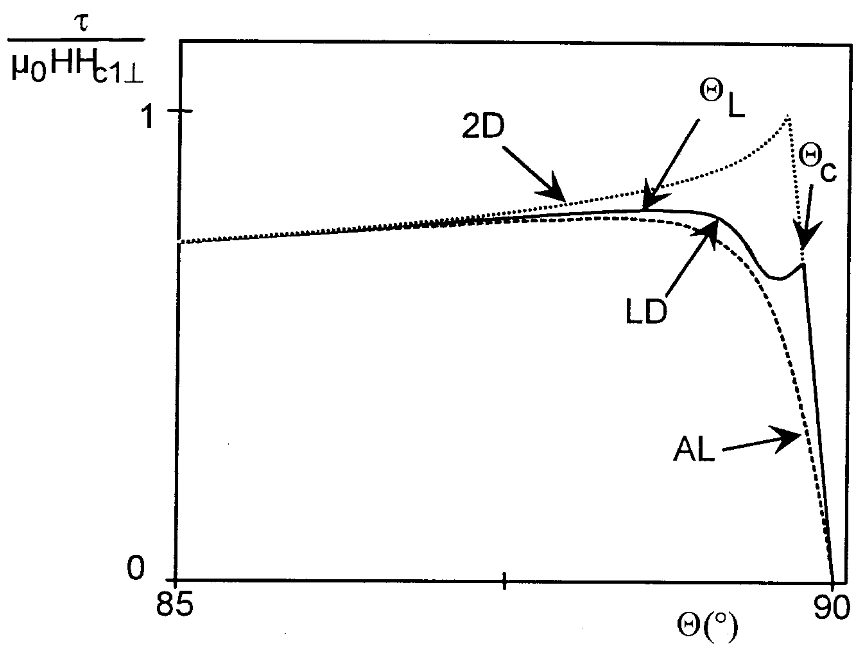

Figure 2.8: Steinmeyer's computation of the torque predicted by the Lawrence-Doniach model at intermediate and high angles for $\lambda_J < \lambda_{||}$. The curve labeled "2D" corresponds to a pure two-dimensional solution ($\gamma = \infty$). "AL" marks the Kogan-London model. "LD" is the Lawrence-Doniach curve. θ_L marks the Kogan-London maximum, and θ_C shows the position of the lock-in transition. This curve is for $\gamma = 100$; for smaller γ the solid and dashed lines follow each other more closely up to the Kogan-London maximum. The figure is reproduced exactly from [7].

reproduced in Figs. 2.8 and 2.9. Figure 2.8 corresponds to the case $\lambda_J < \lambda_{||}$, for which there is no combined or staircase phase. Figure 2.9 corresponds to the case $\lambda_J > \lambda_{||}$, for which there is a combined phase. The jump in this graph is due to a first order phase transition between the tilted and the locked-in phases (see [8]).

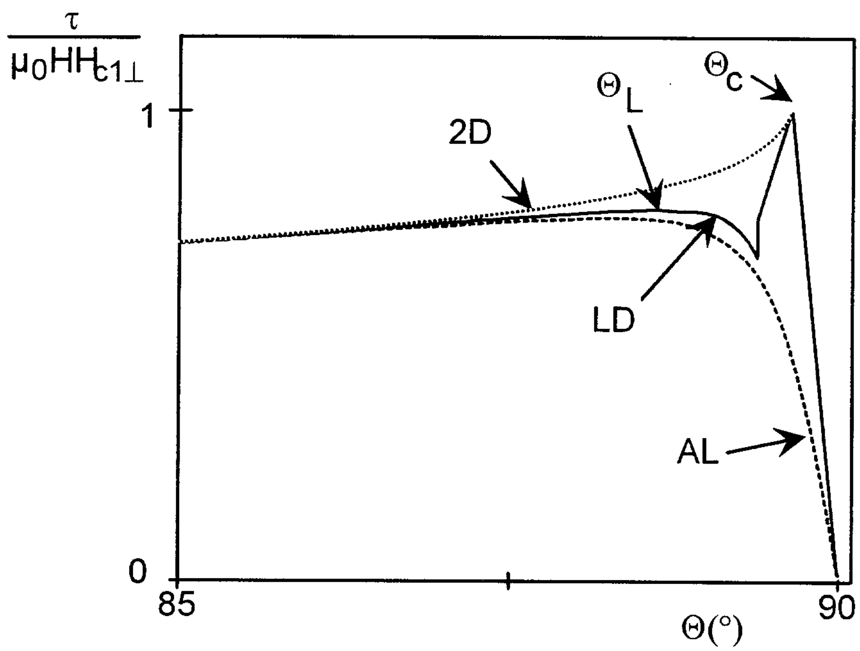

Figure 2.9: Steinmeyer's computation of the torque predicted by the Lawrence-Doniach model at intermediate and high angles for $\lambda_J > \lambda_{||}$. See Figure 2.8 for a description of the symbols. The figure is reproduced exactly from [7].

2.2.6 The Lawrence-Doniach model in the quasi-3D regime

At relatively high temperatures, just below T_c, $Bi_2\,Sr_2\,Ca\,Cu_2\,O_{8+\delta}$ and $Tl_2\,Sr_2\,Ca\,Cu_2\,O_{8+\delta}$ become quasi-three dimensional, as ξ becomes very large near the critical point. This occurs [27] in the temperature region of $T^* = T_c(1 - 2\xi_{||}^2(0)/\Gamma^2 d^2)$, and is less than 1 K from the transition temperature for those two materials. Our experimental measurements did not probe this regime, but we present a brief discussion of this case for completeness.

In the quasi-3D regime the Josephson flux vortices are larger than the interlayer spacing, d. Figure 2.5 shows that this is likely to have a significant effect on the system. The kink length in the staircase flux lines in this regime is larger, $L_K \approx \xi_{||}(T)$, and flux cores extend over several layers.

This case is analyzed in detail in [25]. Feinberg and Ettouhami show that the results are qualitatively very similar to those of the quasi-2D approach, with a lock-in angle, a torque anomaly at high angles, and similar features of the quasi-2D model.

2.2.7 Shortcomings of the Lawrence-Doniach treatment

This treatment models the case of a simple SIS lattice. This differs from the structure of such high-T_c superconductors as $Bi_2Sr_2CaCu_2O_{8+\delta}$ and $Tl_2Sr_2CaCu_2O_{8+\delta}$, in which the two superconducting sheets per unit cell are separated by a fairly small fraction of the total unit cell ĉ-axis height. An ISNSI (or possibly NSNSN in the case of Pb-doped $Bi_2\,Sr_2\,Ca\,Cu_2\,O_{8+\delta}$ [9]) model would be a more accurate representation. In such a treatment the thin layer between adjacent sheets within a cell would be modeled as a normal metal, and the thicker layer between unit cells would be modeled as an insulator or normal metal. Feinberg and Ettouhami expect [25] that this refinement will not significantly alter the qualitative results of the Lawrence-Doniach calculation.

This expectation can be tested by our work. Regi *et al.* have shown [9] that the normal-state resistivity along the ĉ-axis increases by about two orders of magnitude as $Bi_{2-x}\,Pb_x\,Sr_2\,Ca\,Cu_2\,O_{8+\delta}$ is doped from $x = 0$ to $x = 0.4$. As this resistivity is due almost entirely to the resistive nature of the non-superconducting layers in the material, we should expect no qualitative differences in the behaviour of the differently-doped materials if Feinberg and Ettouhami's conjecture is correct.

The Lawrence-Doniach free energy expressions used here and in [7] also make use of the approximation that the $\vec{H}_0 \parallel \vec{B}$ [25]. A more thorough treatment would correct the magnetic flux direction internal to the crystal for shape-dependent demagnetization effects.

2.3 Summary of the theories in relation to the present experimental work

In this work we measure the torques on relatively thick single crystals of $Bi_{2-x}\,Pb_x\,Sr_2\,Ca\,Cu_2\,O_{8+\delta}$ at various dopings, at temperatures significantly lower than T_c, conditions ideal for distinguishing between the Kogan-London and Lawrence-Doniach models as they apply to $Bi_{2-x}\,Pb_x\,Sr_2\,Ca\,Cu_2\,O_{8+\delta}$.

The Kogan-London model predicts for the torque a single-peaked curve, such as in Figure 2.1, for each crystal. We would expect the maximum to shift toward lower angles as the doping is increased, to reflect the expected lower anisotropy factor γ.

The Lawrence-Doniach model predicts a double-peaked curve in most circumstances. The torque would follow Figure 2.1 quite closely up to the maximum and somewhat beyond; Steinmeyer [7] finds that the Lawrence-Doniach maximum essentially coincides with the Kogan-London maximum for $\gamma < 100$.

At higher angles, as the torque is decreasing, the Lawrence Doniach torque would begin to diverge from predicted by the Kogan-London model, being consistently higher than the latter. Eventually, the Lawrence-Doniach torque would increase, possibly discontinuously, and then form a cusp and finally drop linearly to zero torque at $\theta = 90^o$. This cusp marks the lock-in transition.

The only time that the Lawrence-Doniach model would predict a single maximum is when the lock-in transition occurs before the Kogan-London peak. In that case, the torque would increase toward the Kogan-London maximum, then hit a cusp and drop linearly to zero torque at $\theta = 90^o$. This behaviour would be clearly distinguishable from the Kogan-London behaviour, which has no cusp and a significant curvature after the maximum.

It has been shown [22] [33] that the Lawrence-Doniach model applies to the undoped materials. At non-zero dopings it is possible that $\xi_\perp$, the $\hat{c}$-axis correlation length, increases such that the Kogan-London model applies. Whether or not this occurs is one of the questions addressed by this thesis.

It is also worth noting that all experimental analyses of torque data to date have been fitted to the torque predictions of the Kogan-London model. Even those studies which detected clear evidence of Lawrence-Doniach behaviour [7] [22] [33] analyzed their results in the Kogan-London model, making use of the simplifying approximation that the torque maxima in the two models were at the same value of θ. This will probably continue to be the case until such time as a convenient formalism for data analysis under the Lawrence-Doniach model is developed and promulgated.

Chapter 3

Apparatus

3.1 Experiment

In this work we had to measure precisely the differences in the torque in zero magnetic field and in 1 tesla applied field, on small crystals of superconductor at liquid nitrogen temperature. The crystals themselves were delicate, and care had to be taken in their mounting to avoid destroying them.

3.1.1 Torquemeter

The torquemeter used in this work was a modification of a torquemeter originally used by Griessen and described in [34], subsequently modified by Ostapiak [35].

All of the metal parts of the torquemeter are made of Berylco 25, an alloy of beryllium and copper. This material is chosen for its low magnetic susceptibility and for its ability to produce springs which can flex with little

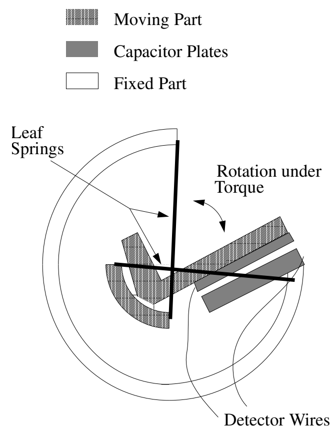

Figure 3.1: The Griessen torquemeter

hysteresis. The torquemeter consists of a fixed and a moving part. The parts are connected by two pair of crossed leaf springs which allow the moving part to rotate under the action of an external torque. A capacitor is formed consisting of one plate on the fixed part and one on the moving part. When the moving part rotates under an external torque the distance between the capacitor plates changes. The change in capacitance can then be measured electronically. Figure 3.1 diagrams the torquemeter from a viewpoint along the rotation axis.

For small torques, resulting in small plate deflections, the deflection of the moving capacitor plate is linearly proportional to the applied torque. The capacitance, equal to $\frac{\epsilon_0 A}{d}$, varies in a linear manner with applied torque for all practical purposes, as $\frac{\Delta d}{d} \approx 10^{-6}$ in our measurements.

The torquemeter was originally designed for measurements of Fermi surface oscillations in noble metals at liquid helium temperatures, with stability, sensitivity, and repeatability requirements which differed from those of our work. The original design called for the probe to hang in a vertical solenoidal magnet. The angle which the magnetic field made with the sample was adjusted by rotating the entire probe head. Torques were measured about a horizontal axis, which was also the rotation axis of the probe head. We found that this approach was not appropriate for our work. The Fermi surface oscillation measurements were fairly insensitive to interference from external causes or from a uniform drift because such interference typically had negligible Fourier components in the interval of interest, while the signals varied sinusoidally. We had no such spectral selectivity over changes in the measured capacitance.

The signals in our experiment were at the limit of detectability in our apparatus, somewhat under 0.1 dyne-centimetres. We found that rotating the probe head through an angle, then returning it to the original angle, introduced a random deviation in the absence of any sample which corresponded to a torque of as much as eighty dyne-centimetres, while our smaller samples could be expected to produce torques on the order of dyne-centimetres. We attribute this deviation primarily to changes in parasitic capacitance as the wires in the torquemeter moved while the probe head rotated. We also expect that some of the effect is due to minute settling of components after rotation, since an extraneous signal of that magnitude can be expected if the mean capacitor plate separation changes by one micron. We further found that rotating the probe head strained the components in such a way that the system required almost two hours to relax to a fairly constant reading.

To circumvent these problems we modified the geometry of the torquemeter. The head was removed and mounted in a fixed orientation, with the torque measurement axis vertical rather than horizontal. By removing all freedom of movement of the fixed parts of the probe head we eliminated strain and rotation-induced drift and random jitter. Since the moving part of the torquemeter has total displacements of less than ten nanometres under the torques experienced in this work, problems with changes in parasitic capacitance due to bending of the wires were also eliminated. To take advantage of this new orientation (see Figure 3.2) we then had to change the geometry of the applied field. We chose to use a horizontal magnetic field which could be rotated independently of the torquemeter.

The new configuration had some weaknesses, primarily due to the fact that this was a probe head designed for one geometry and forced to work in a very different one. The leaf springs now had to support the weight of the moving part of the torquemeter in a direction along the narrow widths of the faces of the springs rather than perpendicular to the faces of the springs, while still responding to torques in the original direction. The springs tended not to bend as smoothly when loaded this way. The readings would occasionally "hang up" for a few minutes, then suddenly move to the expected values. Also, as the cryogen evaporated throughout the course of measurements, the reduced pressure head over the liquid at the bottom of the dewar lowered the boiling point, and hence the temperature, resulting in a steady drift in the reading as

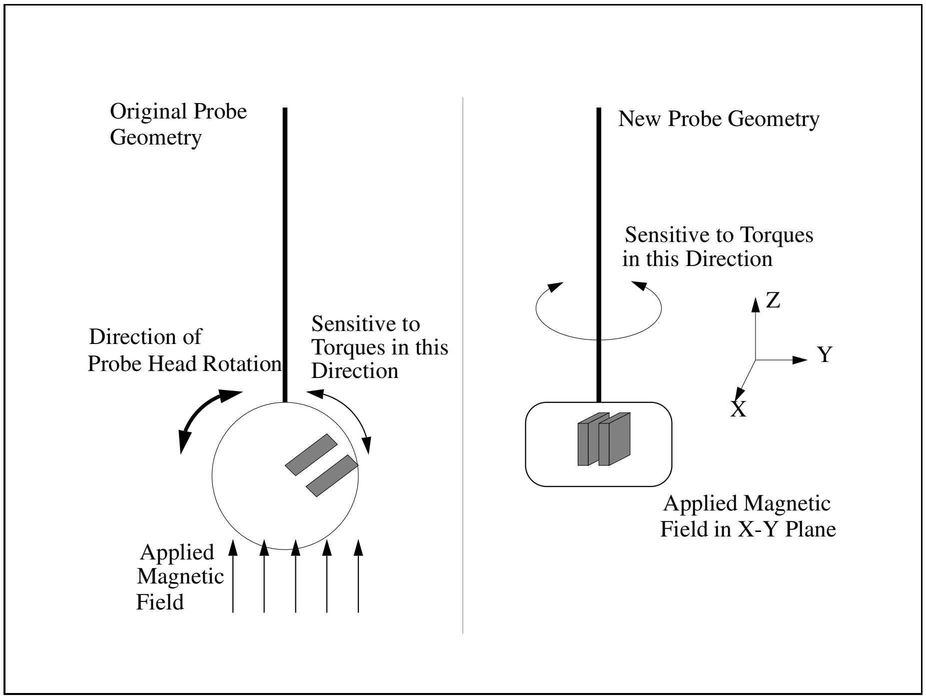

Figure 3.2: The original and new probe head geometries

the probe head cooled. The drift was characterized by a fairly straight, linear ramp with a very low-frequency, apparently random jitter superimposed. The torquemeter was also prone to making irreversible jumps. When this happened the reading suddenly shifted by a moderate amount and remained stable at this new value. Irreversible jumps could move the reading in either direction, and seemed to be correlated with vibration from doors closing or the moving of heavy equipment in other labs or in the corridors.

Because our signals were very small we had to take special pains to eliminate systematic torques not caused by the sample. Even a microscopic sliver of ferrous material would be enough to produce a signal equal in magnitude to that of our samples. We found evidence of such contamination in the angular dependence of background torque readings, and further found that the background changed dramatically every time that the sample holder was mounted on the probe. We attributed this to fragments of tool bits in the threads of the mounting holes on the probe head. All moving metal parts on the probe head were soaked in concentrated hydrochloric acid in an attempt to dissolve away any metallic iron or mild steel which might have been present, though it is more likely that the contamination was from oxides of iron which would be only weakly affected by this acid. Stronger acids could not be used because of the way they attacked the Berylco alloy. We then cleared out the threads of each screw hole in the moving part with a compatible 10-BA drill tap which was thoroughly cleansed in an ultrasonic cleaner before each use. This technique extracted a small amount of machinist's lubricating oil with visible contamination by metallic fragments, probably introduced when the holes were originally tapped. We deduced that the ferrous material in the threads of the screw holes was being reoriented every time that screws were driven into it or removed.

As we could not be sure that the threads were perfectly clean, and could not ensure that the beryllium-copper screws might not pick up a piece of steel from our screwdrivers during routine sample mounting and unmounting, we built a new, nonmetallic sample holder (see Figure 3.3).

This sample holder was machined out of poly-vinyl-chloride (PVC), in two pieces, using thoroughly-cleaned tool bits. After machining, the PVC pieces were washed in concentrated hydrochloric acid and examined under a

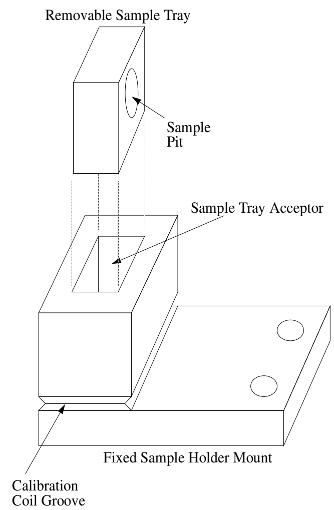

Figure 3.3: The PVC sample holder

dissection microscope at 40× magnification to verify that the machining had not left any slivers of the tool bits in the material. One piece of the new sample holder was attached to the torquemeter with beryllium-copper screws, and not subsequently removed. This part also had a narrow circumferential groove into which was epoxied a single turn of copper wire to act as a calibration coil. The second piece was tapered to slide into a hole in the first and be held in place by static friction. Samples were mounted in a cavity in this second piece, fixed in place by a small spot of Dow Corning brand high vacuum grease silicone lubricant, which becomes hard at liquid nitrogen temperatures. In this way samples could be mounted or removed by disturbing only one non-metallic component of the probe. We found that this modification resulted in a relatively small, reproducible background signal.

Batch	Bi	Pb	Sr	Ca	Cu	Dimensions (mm^3)
BiCu6	2	0	1.88	0.83	1.90	2 x 2 x 0.4
	2	0	1.86	0.61	1.87	
BiCu3	1.92	0.08	1.88	0.82	1.88	2 x 1.5 x 0.3 (#1)
	1.92	0.07	1.93	0.74	1.94	1.5 x 1.0 x 0.3 (#2)
BiCu2	1.89	0.11	1.96	0.95	1.99	1.5 x 1.5 x 0.3
	1.85	0.15	1.81	0.82	1.86	
BiCu5	1.73	0.27	1.80	0.85	1.95	
	1.74	0.26	1.86	0.91	1.95	
BiCu8	1.70	0.30	1.69	1.09	1.93	2 x 2 x 0.4
	1.72	0.28	1.70	1.02	1.85	

Table 3.1: Stoichiometric ratios for $Bi_{2-x}Pb_xSr_2CaCu_2O_{8+\delta}$ specimens from SEM microprobe analysis for two specimens from each batch. Samples used in the experiment were from these batches, but the stoichiometry should be taken only as approximate since there is some variation within a batch.

3.1.2 Samples

The samples which we used in our work were obtained from Dr. John J. Neumeier, of the Condensed Matter and Thermal Physics Group MST-10 at Los Alamos National Laboratory. Several crystals were obtained from each of five different melts with differing lead concentrations; the dimensions were typically 2mm x 2mm in the ab-plane, with the $\hat{c}$-axis thickness between 0.1 and 0.5 mm. Table 3.1 lists the compositions measured by SEM microprobe analysis of two crystals from each batch. The values in the table are normalized to give a Bi+Pb stoichiometry of 2.00, so that the concentrations of Sr, Ca, and Cu are not exactly 2, 1, and 2, respectively.

The $Bi_{2-x}Pb_xSr_2CaCu_2O_{8+\delta}$ samples are orthorhombic (0.1% difference between a and b), but are twinned, so a uniaxial approximation is valid for the bulk properties such as torque.

Samples were chosen for a high volume, and a good appearance. By "good appearance" we mean that the crystal faces should be mirror smooth and should not show facets when used to reflect a light source under a microscope. There also should not be rough, irregular protrusions on the crystal. Such protrusions are usually pieces of non-superconducting flux which are stuck to the crystal, but could contain a superconducting fraction which is not aligned with the main part of the crystal. All of the crystals which gave useful signals were approximately $2 \times 2 \times 0.4\ mm^3$. We were unable to obtain results from any BiCu5 ($x = 0.27$) samples, but we expect that the results would not have provided much additional information over those of the BiCu8 ($x = 0.30$) sample, as the stoichiometries are very similar for the two batches.

Our ideals for sample selection were not always met. The $x = 0.0$ and $x = 0.30$ samples, while large, had poor surface qualities, without mirror smooth faces. The $x = 0.07$ sample #1 had a large irregular lump fused to one face. The $x = 0.07$ sample #2 had visible facets under the microscope. Only the $x = 0.13$ sample had smooth, unfaceted faces.

We did not attempt to perform X-ray diffraction measurements of the samples. Only two of our samples with useful signals had surfaces which showed clean mirror faces. Of those, one had facets visible under an optical examination, and an X-ray examination would have come to the same conclusion. The other smooth-faceted sample was judged of good quality under an optical examination. It was not possible to polish the other samples because of their fragility.

Measurements of c-axis resistance, using fine gold wire and silver paint contacts, were successful in determining the transition temperatures at three concentrations. For $x = 0$ and $x = 0.26$ the transition temperatures were 84 and 85 K, with widths of 2 and 5 K, respectively; the normal state resistivities showed the expected characteristic rise with decreasing temperature above T_c. Transition temperatures ≈ 85 K are typical of unannealed $Bi_2Sr_2CaCu_2O_{8+\delta}$ superconductors. The $x = 0.07$ sample exhibited a much lower, metallic, normal resistivity, and a higher transition temperature ≈ 90 K. The temperature dependence of the normal resistivity, decreasing as the temperature is lowered, suggests an a-b plane conductive path between the front and back contacts, either through a misaligned crystallite inclusion or via silver paint around an edge (some was evident). This complication made it impossible to define a transition width comparable to those of the other two samples, and renders the interpretation of T_c less reliable. Unfortunately, there was not an opportunity to repeat this measurement.

3.1.3 Magnet

All experiments were performed using a Harvey-Wells model L-158 electromagnet. This water-cooled, normal-metal conductor magnet, used in conjunction with the FFC-4 field controller, is capable of producing fields up to 2.1 tesla in a 71 mm air gap, and maintaining the field to within about 2×10^{-5} tesla (*i.e.* a field stability of about 10^{-5}).

The L-158 electromagnet produces a horizontal magnetic field. The magnet can be rotated about a vertical axis, and positioned to within 0.1^{o} using a vernier and an azimuth ring fixed to the base of the magnet.

All measurements were made at 1 tesla to minimize the stress on the thirty year old power supply, and also to reduce the field-ramping time, as long field-ramping times caused some difficulties as outlined in Subsection 3.2.1. The field was ramped up or down at a rate of 0.8 tesla per minute, but was slowed to 0.3 tesla per minute as the field increased past 0.9 tesla.

The rotating-coil gaussmeter attached to the FFC-4 field controller was calibrated with a single-axis Hall effect gaussmeter, rather than a more accurate field-magnitude measurement such as a proton NMR magnetometer, so the absolute value of the magnetic field cannot be known to better than a few percent. This was not considered important because all torque measurements in our work are normalized against the maximum torque value. This inaccuracy does not affect the repeatability of the magnetic field from run to run.

3.1.4 Heat exchange and probe temperature

The probe with mounted sample was enclosed in a stainless steel sleeve. The sleeve was evacuated, then 50 cubic centimetres of helium gas were put into the sleeve to act as an exchange gas (0.03 atm. at room temperature) which would allow the probe to cool fairly quickly when the sleeve was immersed in liquid nitrogen. The probe was then placed inside a long, stainless steel dewar (Minnesota Valley Engineering, Inc. Insert Dewar, serial number 3076) whose dimensions provided the original design criteria for the probe shape.

The dewar was then lifted into the air space of the magnet, and bolted to two steel C-beams which were attached to the walls of the laboratory.

We performed heat exchange calculations which indicated that the temperature of the massive sample holder and sample should be negligibly different from the temperature of the surrounding liquid nitrogen bath. This conclusion was verified to $\sim 0.1\ K$ in a separate measurement using a copper-constantan thermocouple. Variations in temperature due to changes in atmospheric pressure ($\pm 0.2\ K$) and liquid nitrogen hydrostatic head ($\pm 0.2\ K$) were predicted, and the latter effect observed over the time of the measurement. We concluded that the temperature of the samples during our measurements lay in the interval $77.6 \pm 0.3\ K$.

The rate of evaporation of liquid nitrogen in our experiment led to a temperature drift of 10 mK per hour. The resulting capacitance drift in our measurements is consistent with our observed capacitance change due to thermal contraction during the initial cool-down, from 3.6 pF at room temperature to 5.5 pF at liquid nitrogen temperature.

3.1.5 Electronics

Figure 3.4 presents a block diagram of the electronics used to measure torques. The details of the capacitance bridge are presented in Figure 3.5. The oscillator delivers a 90 volt sine wave at 2.275 kHz to the input of the capacitance bridge. The frequency is chosen to minimize the pickup of coherent noise, the dominant source of which is from mains currents appearing at 60 Hz

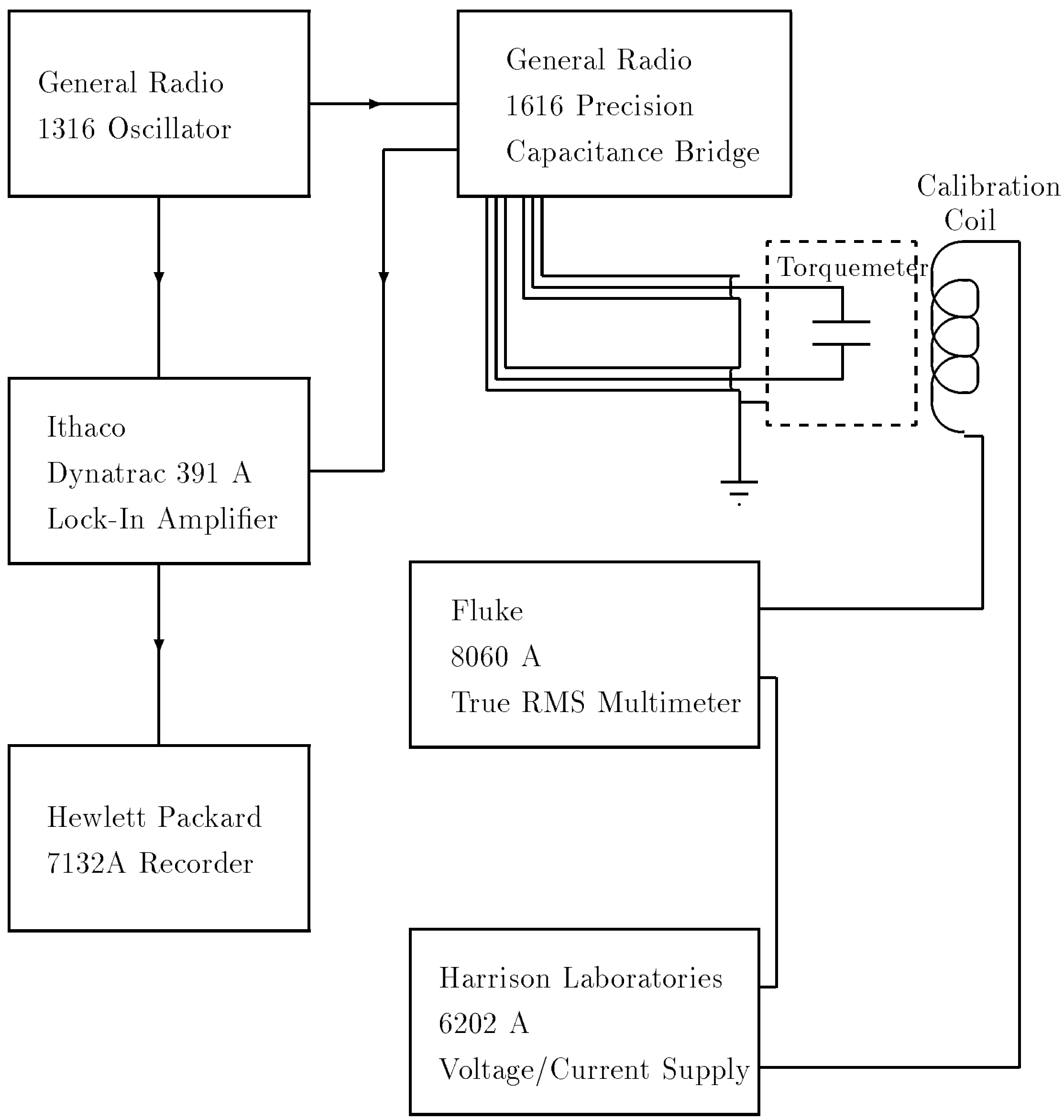

Figure 3.4: Block diagram of torque measurement circuitry

and harmonics. The bridge is balanced by adjusting the voltage on the reference arm of the circuit. When $V_X C_X = V_{Ref} C_{Ref}$, the output is a virtual ground. When this is not true, the output delivers a signal at the carrier frequency whose

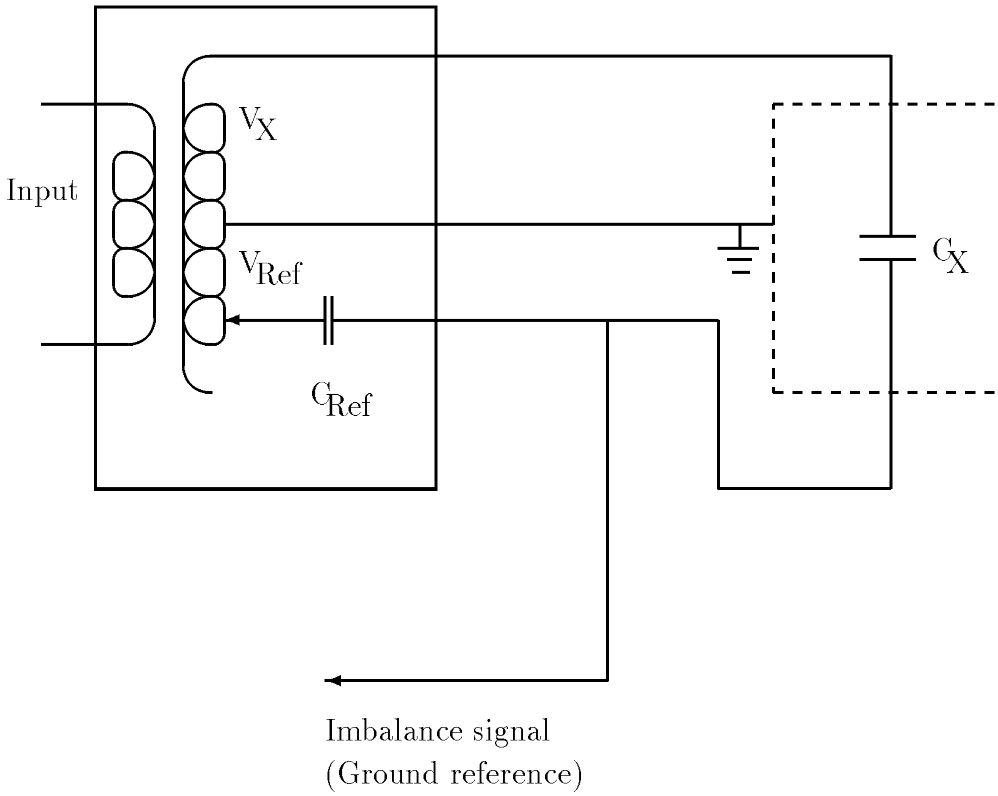

Figure 3.5: Schematic diagram of capacitance bridge

amplitude is strictly proportional to the capacitance imbalance. The linearity of our electronics was verified by introducing a series of progressively larger imbalances on the capacitance bridge and verifying that the output varied linearly with bridge imbalance to our measurement precision. The lock-in detector applies this signal to a demodulator along with a reference signal from the oscillator. The demodulator can be thought of as a gated integrator triggered on the reference signal, or alternately as a mixer, which extracts that component of the signal which is coherent with, and at a particular relative phase to, the reference signal. The lock-in sensitivity was set to $3\mu V$, and a low pass filter on the output was set with a time constant between one and four seconds, depending on the conditions, to filter out noise due to building vibration. The output of the lock-in detector was passed to a chart recorder.

The calibration coil assembly formed an electrically distinct unit. During the actual data acquisition the calibration current leads were removed from the probe since every wire plugged into the probe was a major source of vibration as air currents in the room pushed or pulled them.

Noise levels in our experiment were usually about $1aF$ (10^{-18} Farads), out of a total capacitance of approximately $5pF$. This corresponds to a useful sensitivity of approximately one part in 5×10^6, or a capacitor plate deflection of approximately one angstrom. Most of this noise is electronic, not thermal, and is caused by a defect in the oscillator which introduces random jitter to its output. At times, the oscillator acted according to specification, then no detectable noise passed the low-pass filter on the lock-in amplifier. We did not attempt to repair the oscillator because the dominant source of error in our measurements was not this random noise, but rather the much lower-frequency displacements in the data discussed in Subsection 3.1.1.

3.2 Data acquisition

3.2.1 Data acquisition technique

For our work, we had to measure the torque on a sample due to a magnetic field applied at a known angle to the sample.

The most direct way to measure the torque on the sample would have been simply to rotate the magnet to the appropriate position at zero applied field, measure the capacitance of the torquemeter, then ramp the magnetic field up to the desired value and re-measure the capacitance. The difference in capacitances would then be linearly proportional to the torque on the sample.

The problems mentioned in Subsection 3.1.1 prevent us from collecting data in this way. It takes almost two minutes to ramp the magnetic field up to the value of 1 tesla which was used in this work. During this interval the steady reading drift would result in a different capacitance at the end of the field-ramping interval even in the absence of a true torque. Further, if, during this interval, the reading were to make one of its sudden irreversible jumps, it would corrupt the final capacitance reading. Something as minor as a door closing in another room while the field was ramping could corrupt a reading.

We adopted two data acquisition strategies for use under different conditions. Of course, before anything else could be done, calibrations had to be made. The magnetic field was ramped to 1 tesla at an applied angle of $+2.6^{o}$ as measured on the magnet azimuth ring. The output of the lock-in detector (see Subsection 3.1.5) was passed to a chart recorder rolling at six inches per hour, which then provided a record of capacitance as a function of time. A baseline reading was taken for a few minutes, then a known current was slowly applied to the calibration coil. Over several seconds the current was ramped up to about thirty milliamperes. This resulted in a step in the capacitance. A few minutes later, the current in the calibration coil was gradually reduced to zero. The capacitance stepped back to the vicinity of its earlier value, and was recorded for a few more minutes. Lines were then drawn, one along the chart record with current in the coil, the other through the two zero-current baseline values. If the lines were found not to be parallel we concluded that there had been an irreversible jump in capacitance during this calibration procedure, the reading was discarded, and the procedure repeated until a consistent reading was obtained. The value of the torque was taken to be proportional to the vertical separation of these two lines (see Figure 3.6). Reading that figure from left to right, we began by taking a baseline, then applying a moderate current of approximately 15 mA, and from there increasing the current again to approximately 40 mA, then reducing the current back to zero. We could see that the drift in the 40 mA trace was opposite to that in the baseline readings, so we re-centered the trace on the chart recorder and tried again. The next measurement was made at 17.74 mA, and produced a good reading, with a drift consistent with that in the baseline. We took a second reading immediately afterwards at 39.09 mA to verify linearity and to improve our confidence in the calibration; although the drifts had reversed in direction, the baseline and reading drifts were self-consistent.

Where large signals were expected, exceeding the full-scale deflection on the chart recorder, this procedure was then repeated, but instead of applying a current to the calibration coil, a known capacitance difference was entered on the capacitance bridge, providing a measure of the chart displacement induced by a known change in capacitance. In this way, if the pen went off scale on the

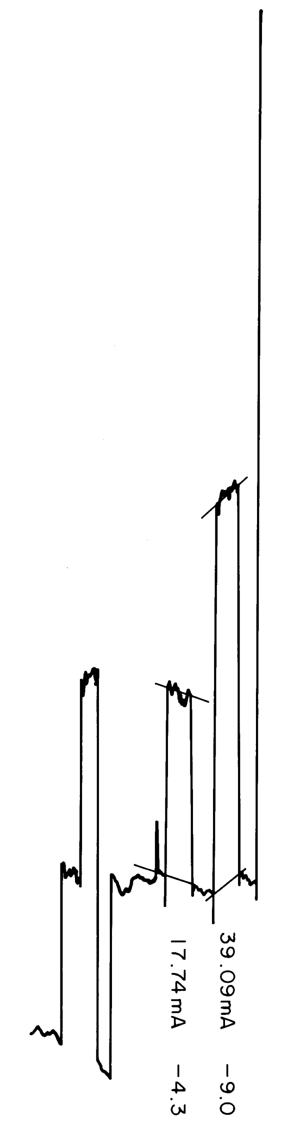

Figure 3.6: Calibration torque readings from the chart recorder. The calibration coil currents are shown alongside the corresponding chart recorder displacements, in chart units (an upward displacement is negative in this diagram). The individual features are described in the text.

chart recorder we could bring it back on scale by changing the capacitance on the bridge, resulting in a known DC shift in the detector.

A similar procedure could now be applied to obtain the torques. We took a baseline at zero field. Next, we would ramp up the magnetic field at a known angle to the sample and record the new detector output level for a few minutes. We could then lower the field again and take a new baseline for a few minutes. Drawing in the two lines as described previously, the displacement between these lines would give the torque on the system at that magnetic field and angle; see Figure 3.7. The sharp peaks in the data are due to the torque exerted on the metal torquemeter because of eddy currents induced by the changing field on the probe head. The field ramps up at a constant rate, producing a linearly increasing torque proportional to $B\frac{dB}{dt}$, until the field reaches its desired value and $\frac{dB}{dt}$ falls quickly to zero, causing the torque to jump discontinuously (on the time scale of the chart recorder tractor feed rate of six inches per hour) to the true sample torque. Reading the figure from left to right, features are characterized as follows. First, there is a baseline region of zero applied field. It is fairly smooth, with some low-frequency jitter. Next, the field is ramped up to its full value in approximately two minutes, producing a linearly increasing torque. When the field reaches one tesla, the field stops ramping, at the cusp. The torque falls rapidly to the true torque reading, represented by 1.2 chart units, at one tesla applied field. A couple of minutes later, the power supply to the magnet is switched to ramp down the field, and the torque jumps quickly to a new value at the second cusp. As the

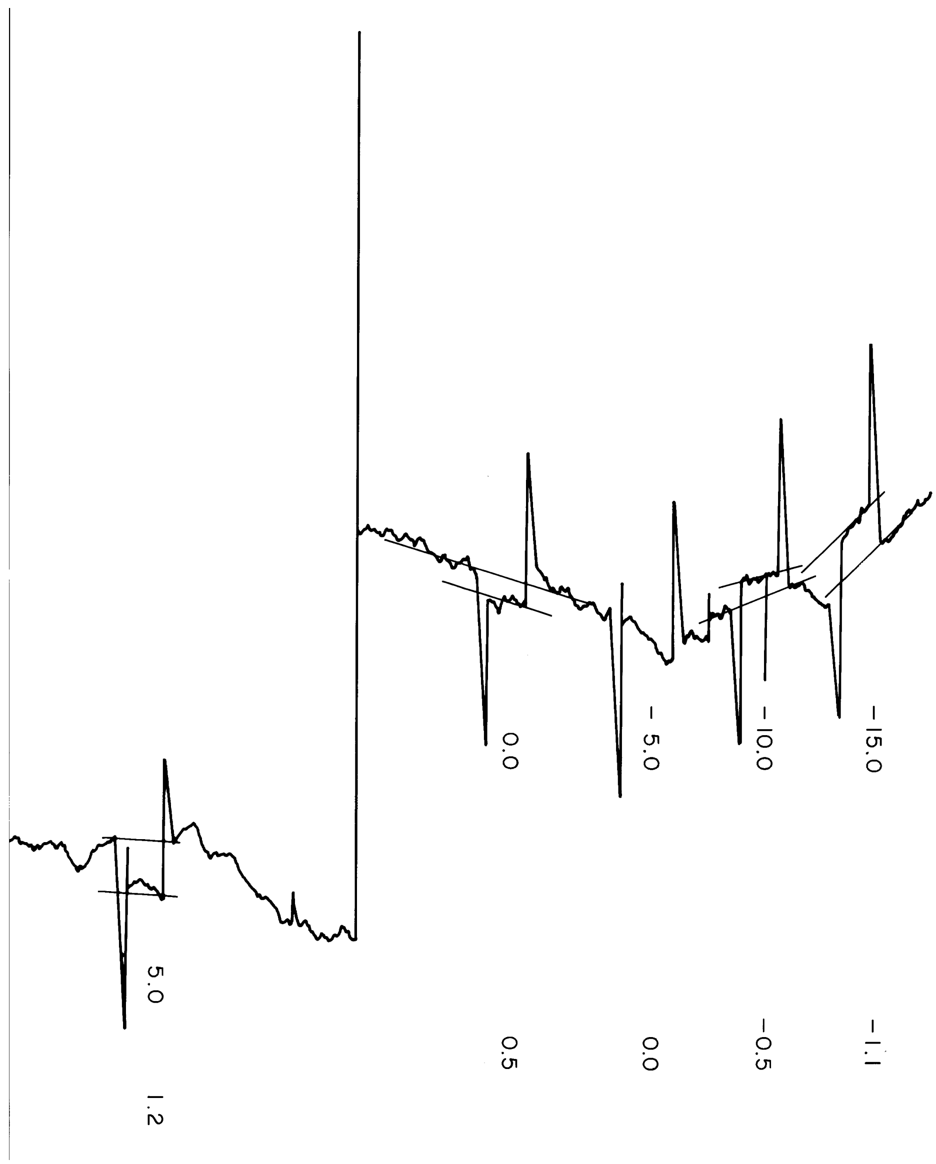

Figure 3.7: Absolute torque measurements from field ramping, at angular intervals of 5^o from $+5^o$ to -15^o. The numbers at the bottom of the figure are the chart displacements, relative to the baseline, which are proportional to torque. The individual features are described in the text.

field ramps down, the torque tends linearly back to its zero-field value. This scenario is repeated for each point.

The $1T$ applied field regions are those regions between cusps which are lined up with the numbers in the figure. The uppermost number is the dialed angle, in degrees, of the magnet on the azimuth ring; the lower number is the distance between the ruled lines, in centimetres, on the original chart paper. The large jump in background reading about a third of the way through the record is due to our changing the bridge settings to center the trace on the chart, as it was drifting too far toward one edge.

In fact, this magnetic field-ramping technique was too slow for us to use it exclusively. Each data point required at least ten minutes per attempt, and we could expect under normal conditions that between one half and two thirds of the attempts would have to be discarded because of irreversible jumps in the capacitance during the field-ramping intervals.

A faster technique was developed. The technique described above was used to obtain absolute torque readings in the angular range over which we expected nearly zero torque. Some three or four points near each torque zero were taken, then a best-fit line was computed to interpolate the position of the true torque zeroes. The zero with the lower $\frac{d\tau}{d\theta}$ was then picked, and the magnet was aligned with that zero. With the magnet at its full 1 tesla field, a baseline was obtained. The magnet was then rapidly rotated to the angle corresponding to the reading we wanted to take. The new value was recorded for a few minutes, then the magnet was returned to the torque zero position, and the baseline taken once again. Once more, two lines were drawn along the chart record, and if consistent the reading was kept; see Figure 3.8.

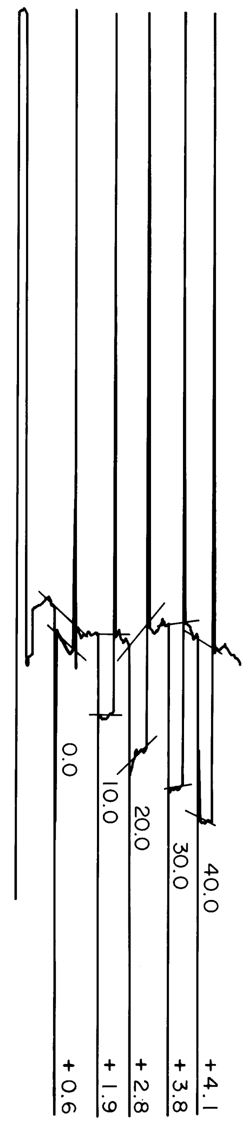

Figure 3.8: Relative torque measurements from field rotation; the labeling is the same as that of Fig. 3.7.

The second baseline from one reading became the initial baseline for the following reading. In this way we could collect a reading every five minutes, and had to discard and re-take no more than one fourth of the readings. This technique allowed us to obtain torques relative to the (zero) initial torque, and also allowed us to observe hysteretic effects if present. One drawback of this technique is that the rotation of a high magnetic field about the irregularly shaped metal moving part of the torquemeter exerts a large torque on the system which overloads the detector for several seconds. During this interval we have no way to notice irreversible jumps or other undesirable excursions which are not caused by the sample. This is not a severe limitation of the technique. A single such displacement would be revealed by an inability to draw parallel lines through the plateau and baseline, and the reading would be immediately discarded. It is also possible that the experiment could make two compensating irreversible jumps, one during each rotation of the magnetic field, resulting in a self-consistent, but wrong, measurement. If this happened, it would only be revealed during the analysis of data, when a point would be seen to be significantly out of place in the context of surrounding points. When we suspected that this may have happened, we recalibrated, then measured the suspect point and the neighbouring points.

3.2.2 Data acquisition runs

A typical data run on a single sample took between one and two days. First, the calibrations were taken. Following this, the torque zeroes were obtained. This took anywhere from three to ten hours depending on the noise conditions within the building. Once the torque zeroes were obtained, a full spectrum of torque data on a crystal took approximately eight hours. Following this, the chart trace was measured and the background subtracted, and the resulting curve examined for any glaring inconsistencies. Any suspect points and their neighbouring points were then remeasured. Once the data was seen to be internally consistent, the probe was taken down, and a new crystal mounted. This took one hour, and the time to settle down during the cool-down took several hours longer.

In the course of this work we made approximately 80 such data runs, most of them before we had detected iron contamination in the sample holder. The results presented in this work represent the data obtained from the final fifteen such runs, all of the runs taken after the effect of the iron contamination was diagnosed and eliminated.

3.3 Sources of Error

3.3.1 Systematic drift

As noted earlier, there was a slow drift in the readings during the course of data collection. In Subsection 3.1.1 we ascribed this drift primarily to the change in the pressure head on the cryogen as the overburden evaporated. The amplitude of the temperature drift was estimated from the phase diagram of liquid nitrogen, and was consistent with that measured with a thermocouple placed within the dewar, approximately 10 mK per hour. Both were in good agreement with the measured change in capacitance due to thermal contraction of the probe head.

The drift error was fairly easy to correct, by the techniques outlined in Subsection 3.2.1. However, there were other, less tractable sources of error.

3.3.2 Crystal ĉ-axis misalignment

Another potential source of error was the possibility that the crystal was not mounted with the ĉ-axis exactly in the horizontal plane. If, instead, the ĉ-axis of the crystal were directed at an angle of elevation θ_e, it would give rise to errors in the measured torque. This error would be particularly severe at low angles, when the field is nominally close to alignment with the ĉ-axis of the crystal. See Figure 3.9. In fact, the true angle between the applied field and the crystal ĉ-axis, θ_T, will differ from the dialed angle on the azimuth ring of the magnet mounting, θ, according to

$$\theta_T = \cos^{-1}(\cos\theta\cos\theta_e). \tag{3.1}$$

Function 3.1 is plotted in Figure 3.10 for a value of $\theta_e = 5^o$, a reasonable upper limit on the mismatch expected in our sample mounting. It is clear that reasonably small misalignments do not contribute significantly to errors in θ_T in the high-angle regime near $\theta = 90^o$.

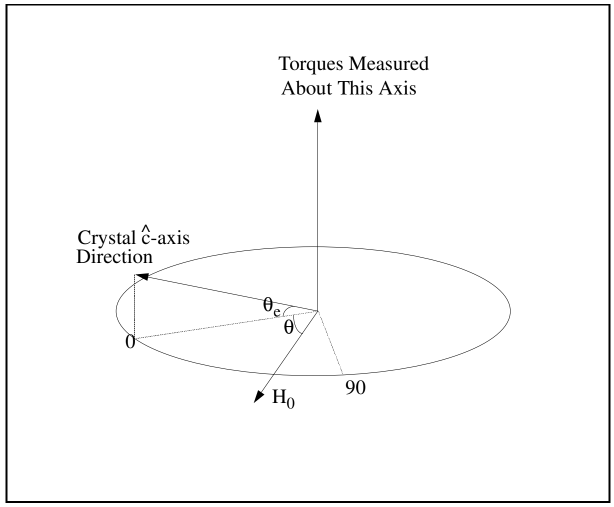

Figure 3.9: Crystal misalignment error geometry

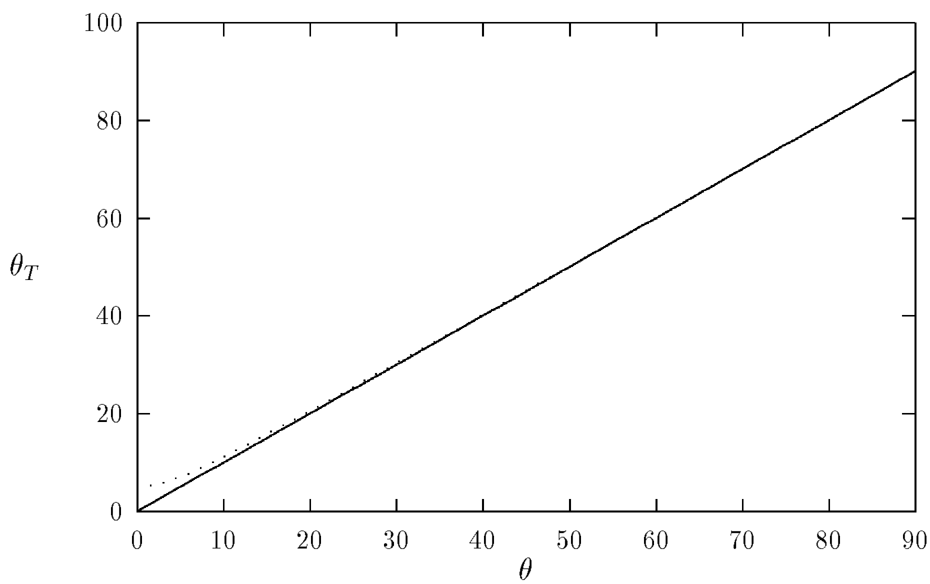

Figure 3.10: Effect of crystal misalignment error of 5^o on field angle: θ_T vs. θ. The solid curve corresponds to perfect alignment.

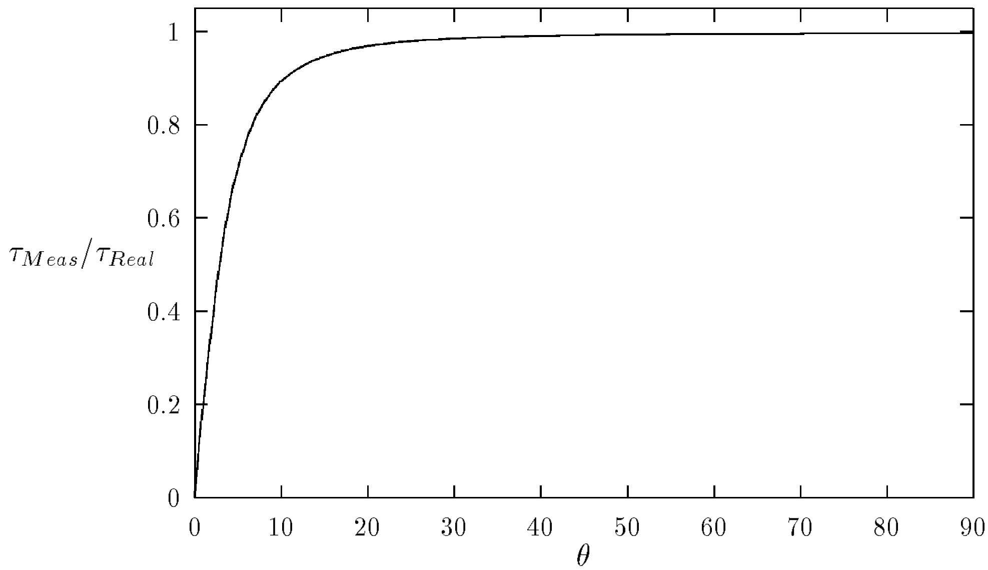

Figure 3.11: Torque correction factor for crystal misalignment

When the crystal is misaligned, the resulting torque will not be maximally projected onto the sensitive axis of the torquemeter. If we assume that the torquemeter is completely insensitive to torques about the other two axes, we conclude that the measured torque is reduced relative to the total real torque by a factor of

$$\tau_{Meas}/\tau_{Real} = \frac{\sin\theta\cos\theta_e}{\sqrt{\sin^2\theta_e + \sin^2\theta\cos^2\theta_e}}. \tag{3.2}$$

Function 3.2 is plotted in Figure 3.11, again for a value of $\theta_e = 5^o$. Once again we see that this error of alignment will have a negligible effect on torque measurements in the high-angle regime. Furthermore, in the low-angle regime, for functions which are close to linearly increasing with angle, this effect largely cancels the angular error described by Equation 3.1. In Figure 3.12 we plot the difference in Equation 2.10, for $\gamma = 10$, between the ideal case of $\theta_e = 0$ and the

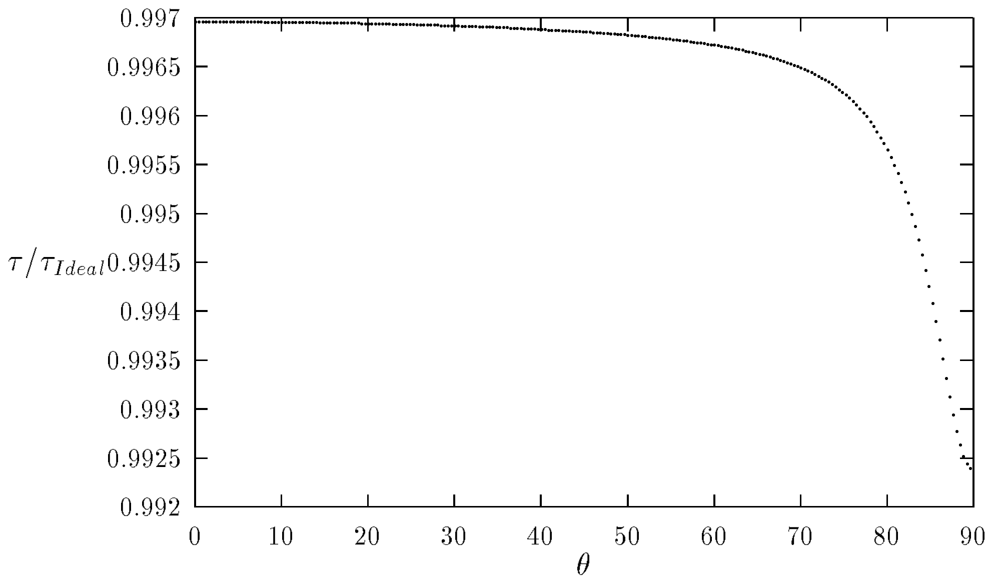

Figure 3.12: Effect of crystal misalignment on data described by Eq. 2.10

case of a misalignment of $\theta_e = 5^o$, taking into account the two effects detailed in equations 3.2 and 3.1. We see from this figure that the error introduced by misalignment is small, less than 0.5% across the entire angular range for $\gamma = 10$.

3.3.3 Probe misalignment

When the probe and sleeve were mounted in the laboratory there was some imprecision in the placement. Because not all bolts were exactly the same diameter as the holes into which they were inserted, the probe's positioning was not repeatable to better than about a one degree rotation. While tighter precision might have been achieved by redrilling holes and replacing the C-beams in the laboratory, the tighter fit would have made it difficult to mount the experiment without risking the safety of the experimenter, or constructing a large, stable mezzanine for the purpose. This imprecision introduces a small error by producing an undetected angular shift in the background during background subtraction. As the background could be fairly accurately modeled by a simple sinusoid with a period of 180^o of azimuth, this would introduce an uncorrected background displacement consisting of a half-wave given by

$$\tau_{uncorrected}(\theta) = 2A\Delta\theta_P \cos 2\theta. \tag{3.3}$$

In Equation 3.3, $\Delta\theta_P$ is the uncertainty in the placement of the probe. The expected amplitude of this error is approximately 1/25 of the background. Because it is not a statistically random error, some care has to be taken in dealing with it. The error is at its largest fairly close to the end points of our sample data, and shifts the high angle readings in a direction opposite to that of the low angle readings. This has the effect of appearing to shift the entire spectrum left or right by a small amount. As the angle of the magnetic field relative to the crystal is inferred from the high-angle torque zero after background subtraction, the error in this inferred angle will be

$$\Delta\theta \approx \tau_{uncorrected}(90^o)\left(\frac{d\tau(\theta)}{d\theta}\right)^{-1} \tag{3.4}$$

For our background and signal amplitudes this correction is approximately 0.1^o in the high anisotropy samples, increasing to about 0.3^o in the relatively low anisotropy samples. We therefore assume these values as uncertainties in the locations of the peaks in our data analysis.

3.3.4 Sensitivity changes

As noted in Subsection 3.1.1, the torquemeter was being used in an orientation for which it had not originally been designed. One effect of this was that its sensitivity, the change of capacitance for a given applied torque, varied quite widely, by up to 30%, over long time scales (days or weeks). Naturally, an undetected change in $\frac{dC}{d\tau}$ would render any data taken hopelessly corrupt. To guard against this possibility, the sensitivity of the apparatus was measured at the beginning of every data run. As a typical run lasted several hours, at various intervals we re-measured a point collected earlier in the run. If this measurement had failed to agree with the earlier value we would have had to discard the entire data run since the last check. Fortunately, this problem never appeared.

3.3.5 Torques in the irreversible regime

At temperatures significantly lower than the transition temperature, $Bi_2Sr_2CaCu_2O_{8+\delta}$ crystals can exhibit a very large irreversible torque due to flux pinning. This torque is typically more than an order of magnitude greater than the strength of the reversible Kogan-London torque. Farrell *et al.* note [15] that torque measurements must be made sufficiently close to T_c to avoid this effect. Iye *et al.* noted that torque measurements [36] in $Bi_2\,Sr_2\,Ca\,Cu_2\,O_{8+\delta}$ were in the reversible regime as much as 6 K below T_c. Our experiments were performed about 7 K below T_c (possibly 12 K for $x = 0.07$). Measurements [37] by Schilling *et al.* of the irreversibility line in $Bi_2\,Sr_2\,Ca\,Cu_2\,O_{8+\delta}$

show that, for $T_c - T \approx 12\ K$, the flux lattice melts when $H_\perp > 0.003T$. Based on this, we estimate that irreversible torques due to flux pinning would only appear at field orientations less than 0.2^o from $\theta = 90^o$, and we must take this possibility into account in interpreting data in this angular range.

Chapter 4

Analysis

4.1 Background characterization

4.1.1 Origins of the background and its expected qualities

In the absence of a sample, the torquemeter produced a non-zero signal under an applied field. This signal had to be characterized so that it could later be subtracted out. The background was measured as a function of the azimuth angle, ϕ, on the magnet, not θ, as the angle to the crystal axis has no meaning when there is no crystal mounted. Since the samples were not always mounted in exactly the same orientation in the sample holder, ϕ and θ are not interchangeable.

We assume that the background torque and the sample torque add linearly. This is certainly a valid assumption, as the metal parts of the torquemeter, responsible for the background reading, are separated by several millimetres from the sample. The sample was itself small, and could have only a negligible effect on the average field direction and magnitude over the metallic parts of the torquemeter. Magnetization effects in the sample, then, are not sufficient to alter the magnetic field to the point that it changes the background profile.

Similarly, the torque on the metallic parts of the torquemeter was small, and the inferred magnetization of the torquemeter is not sufficient to affect the field angle at the crystal by a measurable amount. We can therefore assume that the background and sample torques are simply additive.

The metallic part of the torquemeter is made entirely of beryllium-copper, a low susceptibility alloy. It will exhibit a slight paramagnetism under an applied magnetic field. Because this magnetization reverses when the applied field is reversed, the torque due to this paramagnetism should be periodic in the applied field angle with a period of π radians. We verified that the PVC component contributed negligibly to the background, by measuring the background with the PVC sample holder in place, and again when it had been removed, and saw no measurable change in the background.

If the torquemeter contained any permanently magnetized components which maintained their direction of magnetization even under a $1T$ applied field, the resulting torque would have a period of 2π. We saw no evidence of such behaviour in the background data.

In general, an irregular metal block will have some directions at which an applied field produces a parallel magnetization, and other directions which produce a non-parallel magnetization. The expected torque response can be modeled as sinusoidal, with minor, relatively low frequency perturbations for block shapes which have relatively little short-scale structure. Our torquemeter satisfies this criterion, so we expect to see a background torque resembling a sinusoid with a period of π.

Our measurements of the background supported the prediction that the background torque would be periodic in applied field angle, with a period of π.

4.1.2 Background model

We obtained background data more than once, any time that we made changes to the metallic components of the torquemeter. This was necessary, for instance, when the epoxy attaching the fixed capacitor plate to the probe head failed, allowing the plate to come loose, and requiring that the probe head be disassembled to repair it. After such episodes, the background could be expected to change as not all metallic components would necessarily be returned exactly to their former positions.

In accordance with the reasoning of the last subsection, we have fitted the background data to a sinusoid with harmonics.

A sequence of points, $\{(x_i, y_i) \mid 1 \leq i \leq N\}$, with errors on the y_i's of δ_i, can be fitted by the optimization of linear coefficients, a_j, on a set of linearly-independent basis functions,

$$\{f_j(x)\,|\,1 \le j \le M, M \le N\},$$

in order to minimize χ^2, given by

$$\chi^2 = \sum_{i=1}^{N} \left[\left(\sum_{j=1}^{M} a_j f_j(x_i) - y_i \right)^2 / \delta_i^2 \right] \tag{4.1}$$

The equations minimizing χ^2 are obtained by differentiating χ^2 with respect to the various a_j, and setting these derivatives to zero. This produces the expression

$$\begin{aligned} \mathbf{L}\vec{a} &= \vec{b} && (4.2) \\ L_{ij} &= \sum_{k=1}^{N} \frac{f_i(x_k) f_j(x_k)}{\delta_k^2} && (4.3) \\ b_j &= \sum_{k=1}^{N} \frac{f_j(x_k) y_k}{\delta_k^2} && (4.4) \end{aligned}$$

We solved Equation 4.2 for our background data over the basis of functions: $\{1, \sin 2j\Phi, \cos 2j\Phi\}$. The order of the fit was chosen according to the familiar heuristic that the "reduced χ^2" not be significantly different from 1. The reduced χ^2 is generally $\frac{\chi^2}{N-M}$. If this value is significantly greater than unity it indicates that the fit lies significantly outside the error bars, and so can be considered only a poor fit. If this value is significantly less than unity it indicates that the fit is following the points too closely, well within the error bars, and is probably introducing structure where none exists. For our background data we found that a good match was obtained with a first- or second-order fit. Note that the matrix $\mathbf{L}$ is diagonal in sines and cosines when

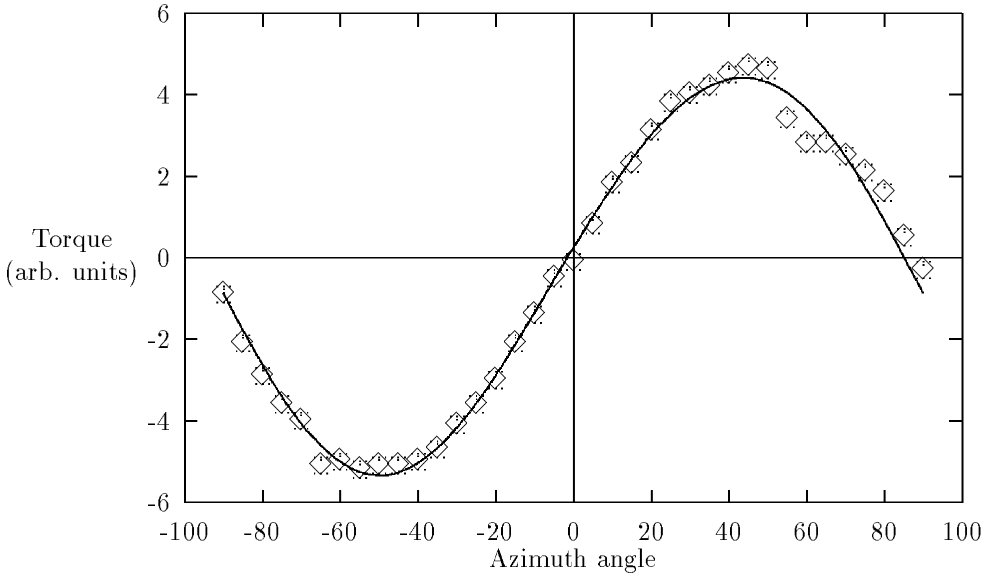

Figure 4.1: Background curve and second-order Fourier fit

the angles are equally spaced over the semi-open interval $[0, 2n\pi)$, but not under other conditions, as these functions are not orthogonal over an arbitrary sequence $\{x_i\}$. A typical background is reproduced in Figure 4.1. The apparent feature near $\Phi = 50^o$ on the azimuth did not appear in all backgrounds, and is likely a statistical anomaly. Because of the geometry of the sample holder, this region corresponds to the region near $\theta = 40^o$, and measurements in that region were not important in the quantitative determination of the final results of this work.

We noticed a significant DC bias in the fits to some background data, caused by the amplitude of the background appearing to be larger in one direction than in the other. This did not seem to come from an intrinsic difference in sensitivity in the probe, as determined by applying positive and negative torques with the calibration coil, but was sufficiently worrisome that we decided to take data with the torque going in a single direction whenever possible. This was not difficult to arrange; by a suitable alignment of the sample holder the sample torque could be made to be the same sign as the background torque over almost the entire interval, with the sign changing only in the relatively unimportant low-angle regime below $\theta \approx 10^o$.

4.2 Our data

The techniques of Subsection 3.2.1 were used to obtain data from each of the five samples listed in Table 3.1. This produced a set of values of torque vs. magnet azimuth angle. Next, the background was subtracted from these data, after being rescaled in accordance with the calibration coil readings. The relative size of background and signal varied significantly from sample to sample. Typically, the background amplitude was between 1/4 and 1/2 of the amplitude of the signal after subtraction, and had the same sign. We interpolated the position of the high-angle true torque zero from these data, and assigned that the value $\theta = 90^o$.

The reproducibility of the data was verified by repeating the high-angle ($80^o < \theta < 90^o$) measurements after first removing and then remounting the samples. In all cases, the data was consistent with the earlier data within the error bars. The sample referred to as "BiCu3 Sample #1" ($x = 0.07$), because of the unusual results obtained the first time, was remeasured twice, once over the full spectrum, and a second time in the high-angle regime. Both remeasurements were entirely consistent with the first data run on that sample.

Steinmeyer *et al.* calculate [22] that the predictions of the Kogan-London model are essentially correct for $\theta \ll \tan^{-1}\gamma$. Even for values of γ as high as 50, the Kogan-London peak occurs more than twice as far from $\theta = 90^o$ as does $\tan^{-1}\gamma$. We can see from Figures 2.8 and 2.9 that the predicted Kogan-London maximum appears at somewhat lower angle than the Lawrence-Doniach maximum for samples with anisotropies of 100 (or greater); however, a quantitative evaluation of this discrepancy is not available in Steinmeyer's thesis. In order to account for this deviation at higher γ, we will, on the basis of an examination of Fig. 2.9, decrease our value of $90^o - \theta_L$ for highly-anisotropic samples ($\gamma \geq 100$) by $20\% \pm 20\%$ before fitting our curves to the Kogan-London equations. We determine the value of γ from the location of the maximum in our data, taking into account the corrections outlined in Subsection 2.1.2. This fitting to the Kogan-London maximum is the usual approach [22] when analyzing data from crystals in the Lawrence-Doniach regime. Very little additional information can be gleaned from the smooth torque increase at low angles up to the maximum, and the region following the maximum does not conform closely with the Kogan-London model prediction. At the same time, the Lawrence-Doniach treatment does not offer a closed-form solution of this intermediate region between the Kogan-London maximum and the lock-in transition. The position of the lock-in transition is itself a strong function of the sample geometry, depending as it does on demagnetizing effects, and the linear torque decrease following the lock-in offers no insight into the magnitude of the anisotropy.

We determined the location of the Kogan-London peaks in our data by fitting three points around the local extremum to a parabola. Error estimates were obtained from the uncertainties in the data, and also the contribution described in Subsection 3.3.3. Given the fairly large uncertainties in our data, no useful extraction of other parameters of the Kogan-London model could be effected by including the low-angle measurements in the fit, but we can be very confident of the locations of the maxima, and of the values of γ required to produce them.

4.2.1 BiCu6 data ($x = 0$)

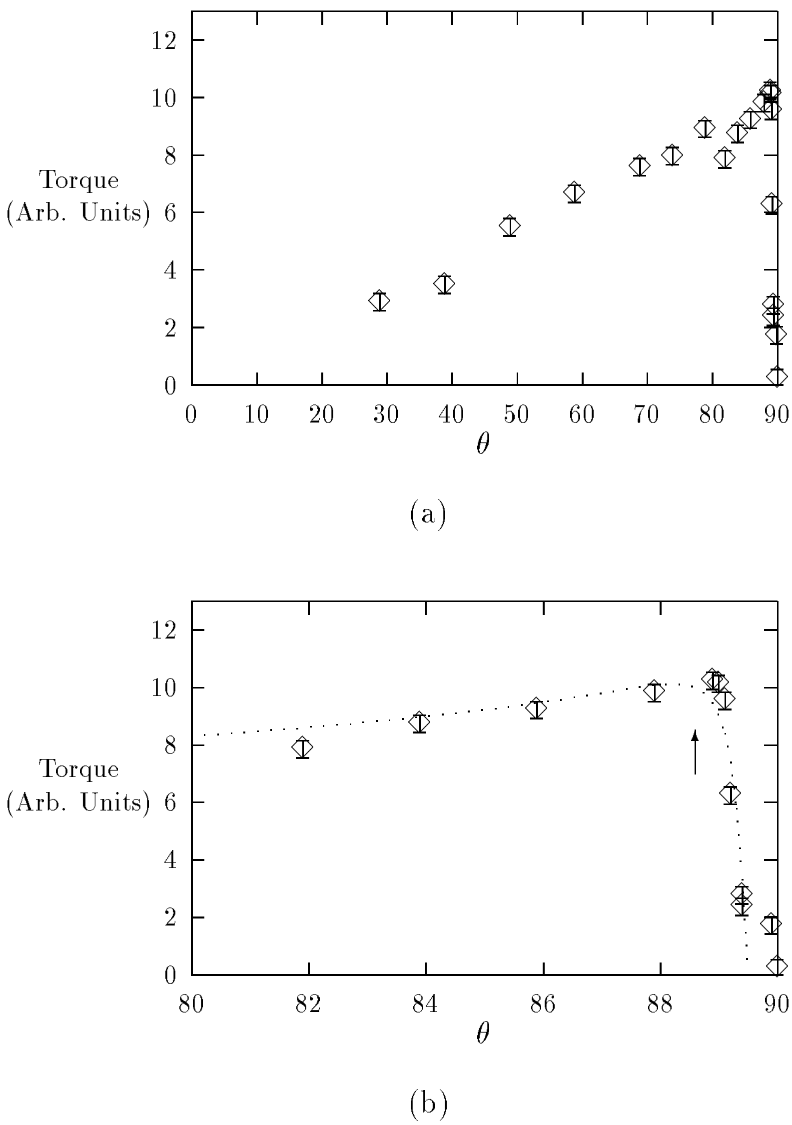

Figure 4.2: (a) Torque data as a function of angle for BiCu6 sample, with Pb concentration $x = 0.0$. (b) shows high-angle detail and a fit from Equation 2.10 to the large peak.

The anomalous feature in the data in Fig. 4.2(b) between 89.5^o and 90.0^o is believed to be due to the presence in our sample of a small second crystalline fragment with a different orientation, rather than a lock-in transition in this angular region. The data are inconsistent with the Lawrence-Doniach predictions for a such a lock-in transition. If a lock-in were to be present, the data for $\theta < \theta_L$ would tend toward the 90^o x-intercept, consistent with the curves of Farrell *et al.* [15], whose very thin samples produce a lock-in transition only unmeasurably close to 90^o. Our data, however, show a clear trend to intersect the $\tau = 0$ axis at an angle $\theta < 90^o$. A linear fit to the data between 89.0^o and 89.4^o extrapolates to an intercept close to 89.5^o. Rather than a lock-in transition, the data suggest two Kogan-London curves, one with an amplitude of 10 units, and a second with an amplitude a bit less than 2 and shifted to the right by about 0.5^o; the torque peak of the smaller crystal would not be resolved on the steep falling edge of the torque of the much larger main crystal. This sample structure is not surprising given the current state of the art in producing such large, thick single crystals. Bent planes, mosaics of small domains, and multiple large components with different orientations are all common problems in the refinement of such crystals. Such a small imperfection is not apparent under the microscope, but its presence is clear from the torque data.

The curve in Figure 4.2(b) is fitted by extrapolating the torque decrease after the large peak to $\theta = 89.5^o$ and then setting this as the new torque zero position for purposes of the fit. As a result of the presence of the second crystal the position of the Kogan-London maximum is uncertain to 0.5^o. This, along with the correction for the difference between the Kogan-London and Lawrence-Doniach peaks at high values of γ, are the dominant sources of error in our estimation of the anisotropy parameter, $\gamma = 100 \pm 25$, for the $x = 0$ sample.

A lock-in transition has been observed in undoped $Bi_2 Sr_2 Ca Cu_2 O_{8+\delta}$ by Steinmeyer [7], [22], and should have been observed in our experiment if our sample had been a perfect single crystal.

It is possible that a lock-in occurs in the interval between 89.5^o and 89.8^o, over which we have no data. However, if the two misaligned crystals of the sample are co-planar we would expect not to see a lock-in transition. A magnetic flux line passing straight through the sample and locked-in in one crystal is quite misaligned in the second crystal, and the lock-in transition is therefore "frustrated", and no longer energetically favourable. Another potential confounding effect is the possibility of irreversible torques being produced in one or the other crystal, which could mask a lock-in signal close to 90^o. Further, while this sample was our largest, and had the highest anisotropy, the signals produced by the sample were fairly small. This indicates that only a relatively small fraction of the sample was actually superconducting. The surface faces were rough, and the signal strength indicated that the sample contained either non-superconducting flux, or voids. In either case, the actual thickness of the superconducting sample could be quite small, implying a large n_{zz}, and hence a lock-in transition which is undetectably close to $\theta = 90^o$.

4.2.2 BiCu3 data ($x = 0.07$)

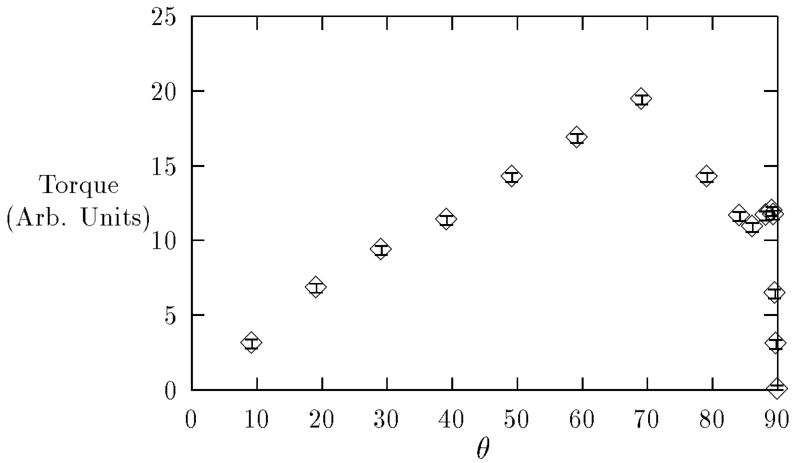

(a)

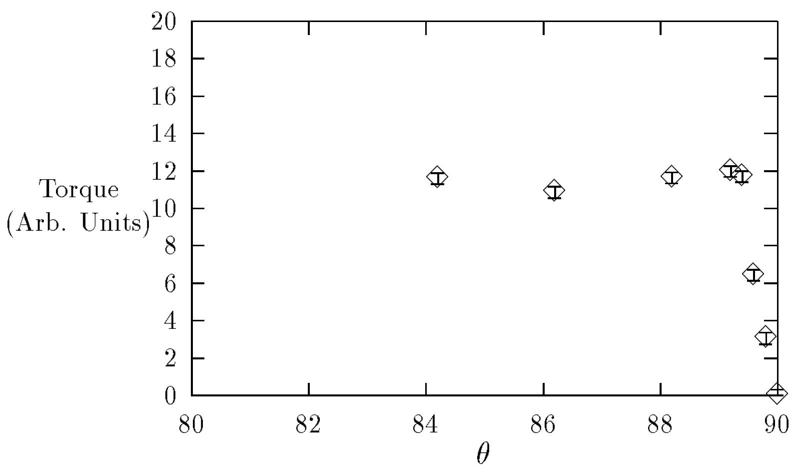

(b)

Figure 4.3: (a) Torque data for BiCu3 sample #1, for Pb / Bi ratio = 0.07 / 1.92. (b) shows high angle detail.

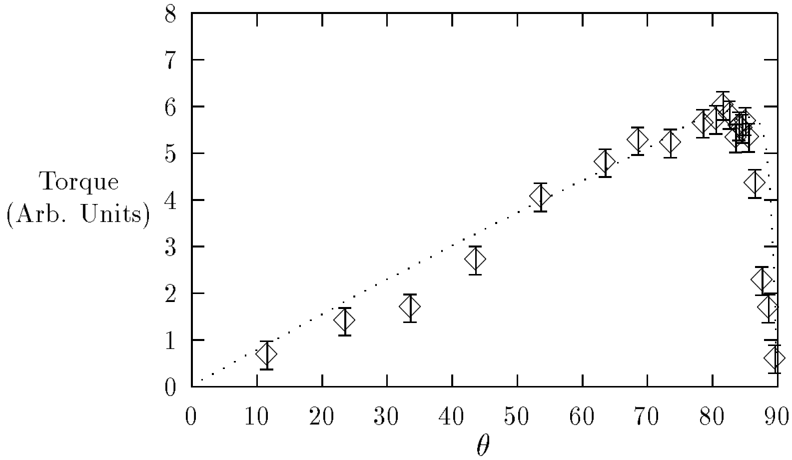

(a)

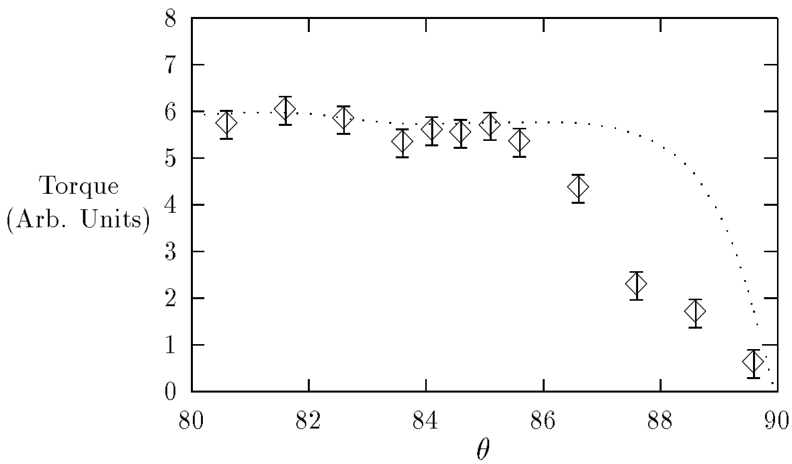

(b)

Figure 4.4: (a) Torque data for BiCu3 sample #2, for Pb / Bi ratio = 0.07 / 1.92. (b) shows high angle detail. The curve fits a simple model of the sample as composed of two perfect crystals, one having a mass of 5% of the total and misaligned by -7.4^o.

We measured two $x = 0.07$ samples in our work. This was the only stoichiometry to give useful signal amplitudes for more than one sample. The first sample we measured, corresponding to "sample #1" in the figure captions, was large but malformed, with a large joined mass and without the mirror faces we would have preferred in a good sample. The data for this sample are presented in Figure 4.3. We were unable to analyze this sample in a way consistent with the other samples in our series, or with other data in the literature. The large peak at $\theta = 70^o$, with no evidence in the neighbouring data points of the broad curvature of a Kogan-London maximum at that point suggests that we are not seeing a true Kogan-London behaviour near there. Our best interpretation of the features in the data is of a second large crystal, more than half the size of the dominant fraction, and aligned at least $5^o - 8^o$ away from it. We can interpret this curve in light of the value of γ estimated from sample #2. The expected increase in torque due to the smaller crystal in the region between $\theta = 70^o$ and $\theta = 85^o$ explains the absence of noticeable curvature in this region due to a Kogan-London peak at 70^o, and the failure of the data in this region to extrapolate to a torque zero near $\theta \approx 80^o$. The torque maximum near 89.5^o, followed by a sharp decrease, indicates a lock-in transition; the orientation of the maximum is consistent with that predicted by Equation 2.20. There is no sign of irreversible torque behaviour, which would appear much closer to $\theta = 90^o$. Because of the uncertainties in the interpretation of this data, we were unable to form any estimate on the value of γ for sample #1. We present this curve because it clearly shows the lock-in transition in a fairly weakly-doped sample. The "frustration" of the lock-in transition does not occur here, as the two crystalline components are not co-planar. Under a dissection microscope the sample appears to consist of an irregular mass attached to one face of an otherwise fairly flat crystal, a geometry which would not prevent a lock-in transition even for severely misaligned crystals.

Once our analysis of the data from sample #1 had shown their unsuitability for extracting useful information, we repeated the measurements on another sample – smaller, but better in appearance, though showing about a dozen facets under the microscope indicating non-parallel crystalline domains misaligned by a few degrees. The data for this sample, referred to in the figure captions as "sample #2", are presented in Figure 4.4. The data show two clear maxima separated by at least 3^o, far from the region of a possible lock-in, and so we have attempted to fit the data by assuming that there are two main crystalline orientations in the sample.

The only way in which a fit could be achieved was to assume that one crystalline component was dominant. By varying γ (assumed uniform), the misalignment angle, and the relative amplitudes, it is possible to produce a curve which fits the data over the entire angular region reasonably well, as shown in Figure 4.4(a). A fairly broad variation in these three parameters is possible while still achieving a fit close to the experimental data, so we can infer only very crudely the value of γ. A fairly good match to the features of the data is produced by setting $\gamma = 35$, the misalignment between 3^o and 8^o, and the amplitude ratio between 0.03 and 0.40. The best fit was found with a separation of 7.4^o and an amplitude ratio of 0.05.

No variation of the parameters would reproduce the data in the region close to 90^o. A collection of small, nearly parallel crystallites would produce a torque curve which was depressed in the high-angle region, consistent with the divergence of the data from the ideal curve plotted in Figure 4.4(b). Such a structure would also prevent any lock-in transition from occurring.

From this analysis, we infer that the anisotropy parameter for this $x = 0.07$ material is $\gamma = 35 \pm 10$.

4.2.3 BiCu2 data ($x = 0.13$)

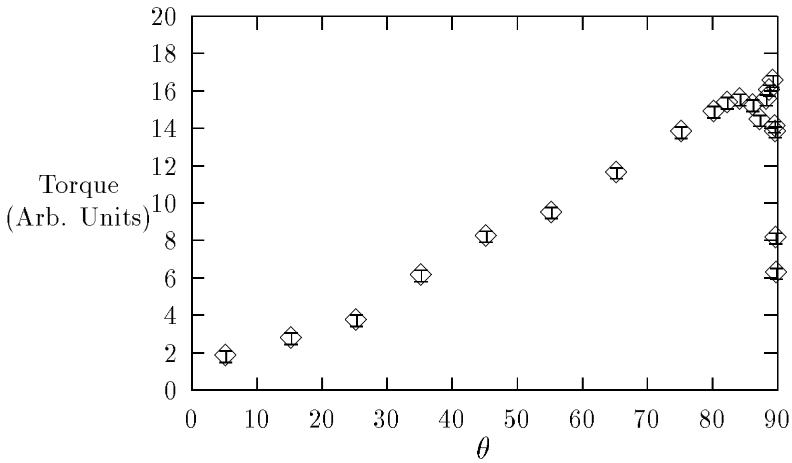

(a)

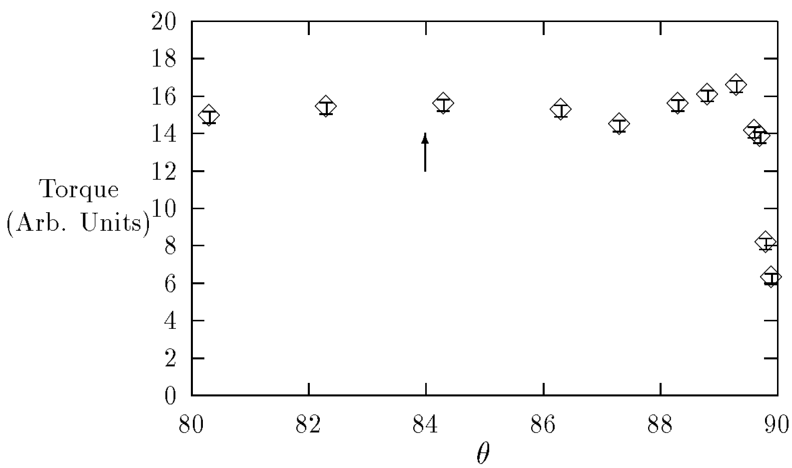

(b)

Figure 4.5: (a) Torque data for BiCu2 sample, for Pb / Bi ratio = 0.13 / 1.87. (b) shows high angle detail. The arrow indicates the position of the Kogan-London maximum.

Referring next to Figures 4.5(a) and 4.5(b), we examine the case of Pb doping $x = 0.13$. This was our sample with the best appearance, and here the data are unambiguous. A Kogan-London maximum is seen in the vicinity of 84^o, yielding our estimate of $\gamma = 24 \pm 2$. A lock-in transition occurs somewhat above 89.3^o, consistent with the estimate from Equation 2.20. Again, no sign of irreversible torque behaviour appears in the high angle data. Our determination of the position of the lock-in transition is limited by our angular resolution, but the signature is clearly present. The data show that the Kogan-London model cannot account for the torque behaviour even in the fairly low-anisotropy $x = 0.13$ sample, and that the Lawrence-Doniach model is more suited for predicting the qualitative behaviour of the torque.

4.2.4 BiCu8 data ($x = 0.30$)

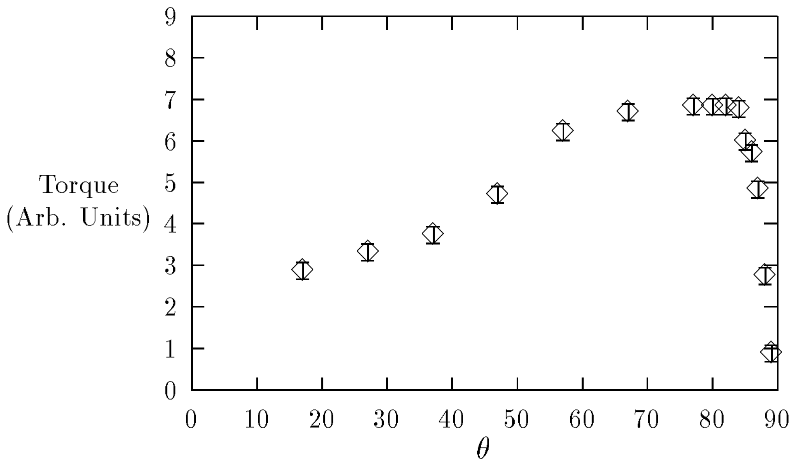

(a)

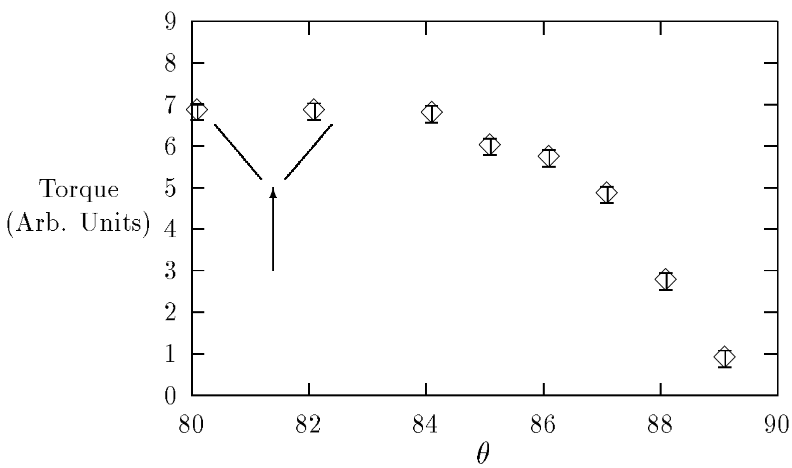

(b)

Figure 4.6: (a) Torque data for BiCu8 sample, for Pb / Bi ratio = 0.30 / 1.70. (b) shows high angle detail. The arrow and lines indicate the position of the Kogan-London maximum, which is quite broad for this heavily doped sample.

Sample	x	θ_L			γ		
BiCu6	0	88.3	$\pm$	0.5	100	$\pm$	25
BiCu3	0.07	81.7	$\pm$	0.2	35	$\pm$	10
BiCu2	0.13	84.0	$\pm$	0.6	24	$\pm$	2
BiCu8	0.30	81.4	$\pm$	1.0	15	$\pm$	4

Table 4.1: Variation of mass anisotropy γ with Pb doping x

Our most highly doped sample was the BiCu8 sample, with $x = 0.30$; the data are shown in Figure 4.6. The Kogan-London maximum is very broad at our measurement resolution, yielding a fairly large error estimate on the anisotropy value of $\gamma = 15 \pm 5$. There is no suggestion of a lock-in transition in our data.

4.2.5 Anisotropies

From the locations of the Kogan-London maxima, we have inferred estimates of the values of γ for these various materials. These values are listed in Table 4.1, and plotted in Figure 4.7.

It is clear that the anisotropy initially falls very rapidly with lead doping, with most of the decrease in anisotropy occuring in the region $x < 0.07$. It is interesting that we do not see evidence of a lock-in transition in the most highly-doped $x = 0.30$ sample. Given the aspect ratio of this sample, we should still easily detect a lock-in transition if it exists and if the sample is a single crystal. The absence suggests either that the highly-doped crystal has crossed over into the three-dimensional regime, or that our sample was of poor quality, and we had coplanar misaligned crystals. More work in this regime, with different, better quality samples, would be very valuable.

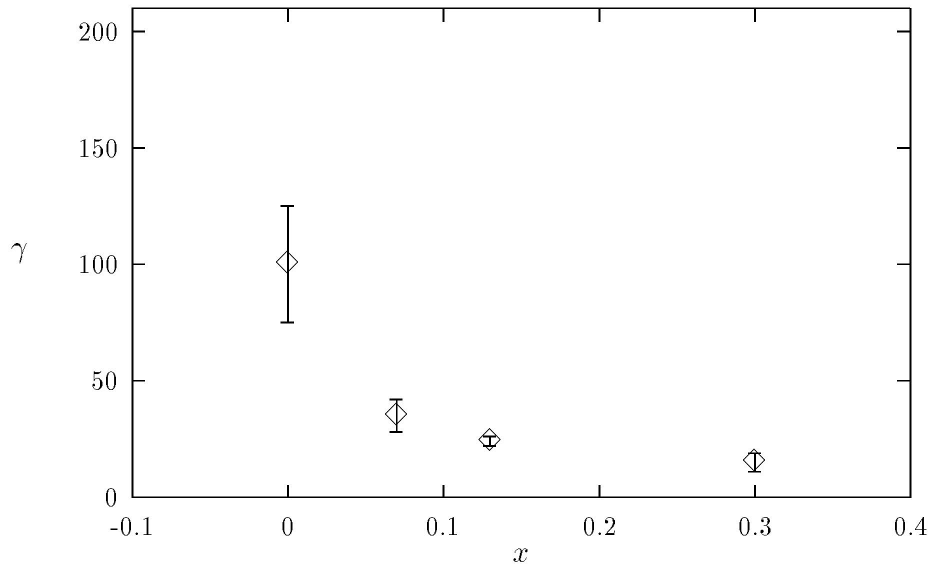

Figure 4.7: Variation of mass anisotropy γ with Pb doping x.

4.3 Resistivity measurements of Régi *et al.*

Régi *et al.* have measured the normal-state resistivity anisotropy, $\rho_\perp/\rho_{||}$, in doped and undoped $Bi_{2-x}\, Pb_x\, Sr_2\, Ca\, Cu_2\, O_{8+\delta}$ [9]. They found that the resistivity anisotropy is approximately two orders of magnitude lower in the compound doped to $Bi_{1.6}\, Pb_{0.4}$ than in the undoped compound, and that the change is mainly due to a decrease in the out-of-plane resistivity. Basov *et al.* [23] studied several families of high-T_c superconductors and have found experimental evidence of a clear relation $\rho \propto \lambda^2$ with the constant of proportionality equal in all tested samples. Assuming a Josephson-coupled model, we conclude on the basis of [38] that the anisotropy parameter γ should vary as the square root of the normal-state resistivity anisotropy, and so we expect it to decrease by one order of magnitude upon doping to $x = 0.40$. This prediction, while not very precise owing to the uncertainty of the resistivity measurements, is supported by our data.

Régi *et al.* also note that a significant increase in $\xi_\perp$ in the superconducting state would cause the system to cross over into an anisotropic 3D regime such as that described by the Kogan-London model, which does not predict a lock-in transition. While the anisotropy $\xi_{||}/\xi_\perp$ is clearly decreased by lead substitution, we have shown in this work that the lock-in persists, and there is no such crossover, for lead dopings up to $x = 0.13$, so the predictions of the Lawrence-Doniach model based on Josephson coupling should still apply in these materials. Our data show no evidence of a lock-in transition in the $x = 0.30$ sample.

Chapter 5

Conclusions and recommendations for future work

We have shown that the effect of lead doping in $Bi_{2-x}Pb_xSr_2CaCu_2O_{8+\delta}$ on the effective mass ratio, γ, as deduced from torque measurements, is to lower it by approximately an order of magnitude, from approximately 100 to 15, as x varies from 0 to 0.3. We have shown that most of this change in the effective mass ratio occurs in the region $x < 0.07$.

We have also shown that the torque behaviour in the doped materials, up to $x = 0.13$, as has been previously shown in the undoped, shows evidence of a lock-in transition, and so strongly suggests that the ĉ-axis correlation length is smaller than or comparable to the ĉ-axis unit-cell length in these samples. Consequently, the superconductor is appropriately described by the Lawrence-Doniach model, treating the material as a lattice of superconducting planes separated by insulating spacers, coupled by Josephson tunneling. It is not sufficient in principle to treat these materials in an anisotropic London-type model such as that of Kogan, though the predictions of that model closely match those of the Lawrence-Doniach model at moderately low anisotropies with very thin samples. This failure of a three-dimensional London model to account for the behaviour of high-T_c materials has been previously shown [7] [22] to hold for undoped $Tl_2\,Sr_2\,Ca\,Cu_2\,O_{8+\delta}$, and in lower anisotropy materials [23] [24] at sufficiently low temperatures. Generally, those high-T_c materials known at present with anisotropies $\gamma \gtrsim 20$ are now seen to behave in a way consistent with the predictions of the Lawrence-Doniach model except just below the transition temperature ($T_c - T \lesssim 0.5\ K$). The lower anisotropy materials are known to behave in a way consistent with an anisotropic London model over a somewhat wider temperature range, but no high-T_c superconductor has shown strong evidence of three-dimensional behaviour to arbitrarily low temperatures.

The Kogan-London model is still of practical use in moderately anisotropic materials outside of the lock-in regime, because of the ease with which the computation yields a valid estimate of γ. We have described a refinement to the analysis of experimental data under the Kogan-London model which acts to lower the estimates of γ for all published torque experiments on highly-anisotropic superconductors.

Future work in this area should include a detailed study of the low-doping region, between $x = 0$ and $x = 0.07$, to determine just how rapidly the anisotropy is suppressed, and to establish better limits on the value of γ in the $x = 0.07$ material. Measurements on high quality single crystal samples with

$0.13 < x < 0.30$ ought also to be made in order to establish convincingly the presence or absence of a lock-in transition at higher dopings, as its absence would indicate the presence of a crossover into the anisotropic Kogan-London regime; our experiments show no evidence of a lock-in at $x = 0.30$ and hence suggest that a crossover has occurred in the interval $0.13 < x < 0.30$. At this time, we do not have access to the samples required to carry out the proposed work.

A calculation paralleling Steinmeyer's [7] should be undertaken to show how the effect of sample magnetization on the direction of magnetic flux internal to the material changes the predicted variation of torque with angle under the Lawrence-Doniach model.

Normal-state resistivity measurements similar to those of Régi *et al.* ought to be made on samples of intermediate lead doping to confirm that the anisotropy measured in this way agrees with the results we have seen in this work. While these measurements are very imprecise, they ought at least to be able to confirm qualitatively the rapid drop in anisotropy at low lead dopings.

A further possibility, for non-zero dopings and fairly large crystals, is to examine the torque behaviour at higher temperatures, to look for a crossover into the Kogan-London regime as the value of $\xi_\perp$ diverges. This will probably not be possible in the undoped material, as the crossover is expected about $0.5\ K$ below T_c, where the torque signal will be too weak to produce reliable signals. At higher dopings we might expect $\xi_\perp$ to be larger at all temperatures, by analogy with the increase in the resistivity ratio, so a crossover might be detectable. This would provide indirect information on the variation of $\xi_\perp$ with lead doping.

Bibliography

[1] J. G. Bednorz and K. A. Müller, Z. Phys. B **64**, 189 (1986).

[2] M. K. We *et al.*, Phys. Rev. Lett. **58**, 908 (1987).

[3] Z. Z. Sheng and A. M. Hermann, Nature **332**, 138 (1988).

[4] H. Maeda, Y. Tanaka, M. Fukutomi, and T. Asano, Japan J. Appl. Phys. **27**, L209 (1988).

[5] V. G. Kogan, Phys. Rev. B **24**, 1572 (1981).

[6] W. E. Lawrence and S. Doniach, in *Proceedings of the 12th International Conference on Low Temperature Physics*, edited by E. Kanda (Keigaku, Tokyo, 1971), pp. 361–362.

[7] F. Steinmeyer, Ph.D. thesis, Technischen Universität München, 1994.

[8] L. N. Bulaevskiĭ, M. Ledvij, and V. G. Kogan, Phys. Rev. B **46**, 366 (1992).

[9] F. X. Régi *et al.*, IEEE Transactions on Applied Superconductivity **3**, 1190 (1993).

[10] V. G. Kogan, Phys. Rev. B **38**, 7049 (1988).

[11] F. London, *Superfluids* (Wiley, New York, 1950), Vol. 1.

[12] F. London and H. London, Physica **2**, 341 (1935).

[13] J. R. Schrieffer, *Theory of Superconductivity* (W. A. Benjamin, New York, 1964).

[14] L. J. Campbell, M. M. Doria, and V. G. Kogan, Phys. Rev. B **38**, 2439 (1988).

[15] D. E. Farrell *et al.*, Phys. Rev. Lett. **63**, 782 (1989).

[16] D. E. Farrell *et al.*, Phys. Rev. Lett. **61**, 2805 (1988).

[17] K. E. Gray, R. T. Kampwirth, and D. E. Farrell, Phys. Rev. B **41**, 819 (1990).

[18] D. E. Farrell, J. P. Rice, D. M. Ginsberg, and J. Z. Liu, Phys. Rev. Lett. **64**, 1573 (1990).

[19] L. Fruchter and I. A. Campbell, Phys. Rev. B **40**, 5158 (1989).

[20] B. Janossy, H. Kojima, I. Tanaka, and L. Fruchter, Physica C **176**, 517 (1991).

[21] K. Okuda *et al.*, J. Phys. Soc. Jap. **60**, 3226 (1991).

[22] F. Steinmeyer, R. Kleiner, P. Müller, and K. Winzer, Physica B **194-196**, 2401 (1994).

[23] D. N. Basov, T. Timusk, B. Dabrowski, and J. D. Jorgensen, Phys. Rev. B **50**, 3511 (1994).

[24] T. Shibauchi *et al.*, Phys. Rev. Lett. **72**, 2263 (1994).

[25] D. Feinberg and A. M. Ettouhami, Int. Jour. of Modern Phys. B **7**, 2085 (1993).

[26] S. Theodorakis, Phys. Rev. B **42**, 10172 (1990).

[27] P. H. Kes, J. Aarts, V. M. Vinokur, and C. J. van der Beek, Phys. Rev. Lett. **64**, 1063 (1990).

[28] L. N. Bulaevskiĭ, Sov. Phys.-JETP **37**, 1133 (1973).

[29] J. R. Clem, M. W. Coffey, and Z. Hao, Phys. Rev. B **44**, 2732 (1991).

[30] S. Doniach, in *The Los Alamos Symposium - 1989 High Temperature Superconductivity Proceedings*, edited by K. S. Bedell *et al.* (Addison-Wesley, Redwood City, 1990), pp. 406–432.

[31] J. A. Osborn, Phys. Rev. **67**, 351 (1945).

[32] L. N. Bulaevskiĭ, Phys. Rev. B **44**, 910 (1991).

[33] J. C. Martínez *et al.*, Phys. Rev. Lett. **69**, 2276 (1992).

[34] R. Griessen, M. J. G. Lee, and D. J. Stanley, Phys. Rev. B **16**, 4385 (1977).

[35] O. Z. Ostapiak, Ph.D. thesis, University of Toronto, 1993.

[36] Y. Iye *et al.*, Physica C **199**, 154 (1992).

[37] A. Schilling, R. Jin, J. D. Guo, and H. R. Ott, Phys. Rev. Lett. **71**, 1899 (1993).

[38] T. R. Chien *et al.*, Phys. Rev. B **50**, 9627 (1994).